SECURITY CLASSIFICATION OF THIS PAGE (When Data Entered)

REPORT DOCUMENTATION PAGE

READ INSTRUCTIONS BEFORE COMPLETING FORM

1. REPORT NUMBER (6) Reports in Meteorology and Oceanography [redacted] Number 2.	2. GOVT ACCESSION NO. / 3. RECIPIENT'S CATALOG NUMBER
[redacted] Momentum and Mass Transfer in a Neutral and Stratified Turbulent Shear Flow.	5. TYPE OF REPORT & PERIOD COVERED (9) Progress Report,
	6. PERFORMING ORG. REPORT NUMBER
7. AUTHOR(s) (10) G.A. Seaver	8. CONTRACT OR GRANT NUMBER(s) (15) N00014-67-A-0298-0011, NR083-201 (16) NR-083-201
9. PERFORMING ORGANIZATION NAME AND ADDRESS Harvard University / Cambridge, Mass. 02138	10. PROGRAM ELEMENT, PROJECT, TASK AREA & WORK UNIT NUMBERS (12) 74 p.
11. CONTROLLING OFFICE NAME AND ADDRESS (11) Office of Naval Research Arlington, Virginia 22217 CODE 480	12. REPORT DATE Jun[redacted]76 / 13. NUMBER OF PAGES 71
14. MONITORING AGENCY NAME & ADDRESS (if different from Controlling Office)	15. SECURITY CLASS. (of this report) / 15a. DECLASSIFICATION/DOWNGRADING SCHEDULE

16. DISTRIBUTION STATEMENT (of this Report)

Approved for public release and sale: distribution unlimited.

17. DISTRIBUTION STATEMENT (of the abstract entered in Block 20, if different from Report)

18. SUPPLEMENTARY NOTES

19. KEY WORDS (Continue on reverse side if necessary and identify by block number)

MOMENTUM AND MASS TRANSFER IN A NEUTRAL AND STRATIFIED TURBULENT SHEAR FLOW.

20. ABSTRACT (Continue on reverse side if necessary and identify by block number)

A fully developed, two dimensional turbulent flow is established in a water channel with a free surface. The unstratified case is first examined in regards to requirements for two dimensionality, steady state, and properties near the free surface with hot film anemonetry. The flow is then stratified by injecting saturated salt water at mid depth. Downstream from the salt injector in the test section the properties of the flow are then examined. Cross sections in the center of the channel one foot apart are taken of the mean and streamwise fluctuating velocities as well as the mean density profiles.

DD FORM 1 JAN 73 1473 EDITION OF 1 NOV 65 IS OBSOLETE S/N 0102-014-6601

-over--

SECURITY CLASSIFICATION OF THIS PAGE (When Data Entered)

163 130

20. Abstract - Cont.

This information along with the boundary conditions of the stress at the wall and the pressure gradient at the wall are then fed into the numerical program of the first integral of the equations of motion. This yields the momentum and salinity fluxes, as well as the inertial terms and pressure gradient as a function of depth and the local Richardson Number. The salinity flux and Austausch coeffiecient behave with the expected reciprocal relationship to the Richardson Number. The momentum results do not. The flow exhibits internal regimes in which the dynamics are different. In the lower region of the flow the turbulent momentum flux is negative, u' and w' are either both positive or negative, and the mean gradient steepens in the streamwise direction. Also the turbulent momentum flux is balanced by the mean advective fluxes. The possibility of the critical layer mechanism transferring momentum from internal waves to the mean flow is considered in the last section. In the upper region of the flow the turbulent momentum flux is positive and is balanced by the vertical integral of the streamwise density gradient. The momentum Austausch coefficient is large as is the local Richardson Number. This is probably due to the fact that the local Richardson Number, as defined, does not properly assess the turbulent kinetic energy available for mixing. Energy is advected into the region as the flow is developing.

REPORTS IN METEOROLOGY AND OCEANOGRAPHY

Number 9

MOMENTUM AND MASS TRANSFER IN A NEUTRAL AND STRATIFIED TURBULENT SHEAR FLOW

G.A. Seaver

 The research was sponsored by The Office of Naval Research under O.N.R. Contract No. N00014-67-A-0298-0011, NR083201.

Division of Engineering and Applied Physics

Harvard University

ABSTRACT

A fully developed, two dimensional turbulent flow is established in a water channel with a free surface. The unstratified case is first examined in regards to requirements for two dimensionality, steady state, and properties near the free surface with hot film anemometry. The flow is then stratified by injecting saturated salt water at mid depth. Downstream from the salt injector in the test section the properties of the flow are then examined. Cross sections in the center of the channel one foot apart are taken of the mean and streamwise fluctuating velocities as well as the mean density profiles. This information along with the boundary conditions of the stress at the wall and the pressure gradient at the wall are then fed into the numerical program of the first integral of the equations of motion. This yields the momentum and salinity fluxes as well as the inertial terms and pressure gradient as a function of depth and the local Richardson Number. The salinity flux and Austausch coefficient behave with the expected reciprocal relationship to the Richardson Number. The momentum results do not. The flow exhibits internal regimes in which the dynamics are different. In the lower region of the flow the turbulent momentum flux is negative, u' and w' are either both positive or negative, and the mean gradient steepens in the streamwise direction. Also the turbulent momentum flux is balanced by the mean advective fluxes. The possibility of the critical layer mechanism transferring momentum from internal waves to the mean flow is considered in the last section. In the upper region of the flow the turbulent momentum flux is positive and is balanced by the vertical integral of the streamwise density gradient. The momentum Austausch coefficient is large as is the local Richardson Number. This is probably due to the fact that, the local Richardson Number as defined, does not properly assess the turbulent kinetic energy available for mixing. Energy is advected into the region as the flow is developing.

1. Introduction

One area of oceanography that has attracted considerable attention is the existence of seasonal thermoclines, main or permanent thermoclines, and small scale microstructure or layering. This paper is concerned with one mechanism that might be responsible for these phenomenon; that is, the effect upon shear-induced turbulence of a stable density gradient.

A fully developed, two dimensional classical turbulent flow is established similar to that of Laufer (1951) and is then stratified by injecting saturated salt water into it. This approach was suggested by the experiments of Ellison and Turner (1960), although it has been significantly extended in parameter space. Because the state of technology prevented them from including advection, which is central to the dynamics, their small bulk Richardson Numbers, and their small aspect ratio (their flow is not two dimensional), their results are preliminary, and the interesting features of this experiment are missed.

In the test section, which is sufficiently downstream of the injecting device to avoid its effect, profiles of $\rho(z)$, $\bar{U}(z)$ and $\sqrt{\overline{u^2}}(z)$ are taken at cross sections one foot apart. This information along with the boundary conditions of wall stress and the pressure gradient at the wall are fed into a numerical computer program of the first integral of the equations of motion. From this the momentum and mass fluxes as well as the advective and pressure gradient terms and local Ri. No. as a function of the normalized depth are obtained for various overall Ri. Nos. The conservation of mass across the two sections is also determined as a check on the results.

Unfortunately in attempting to model oceanographic mechanisms in the laboratory, compromises were necessary. The ocean currents exhibit quite large Re. Nos. and Ri. Nos. In going from the ocean to the laboratory, the physical scale changes by several orders of magnitude. For a constant Re. No., the Ri. No. goes as the cube of this physical scale. For this reason the Re. No. was limited to $\sim$10,000 and the range of the bulk Ri. No. was up to $\sim$0.40.

2. Experimental Apparatus and Procedures

a) The Water Channel

A twenty-six foot plastic flume, eight inches wide, was constructed, supported by wooden frames, The object was to create in the neutral case a fully developed, two dimensional, steady state turbulent flow, the analog of Laufer's wind tunnel experiment, (1951), which he thoroughly investigated. In this turbulent system the turbulent energy goes through all of its stages of transformation across the channel section - turbulent energy production from the mean flow, energy diffusion, and turbulent and laminar dissipation. From the test section the flow proceeds over a dam at the channel's end. This controls the depth of the flow for a fixed flow rate and flow rate Re.No. The fluid then recirculates through a 2000 gallon sump which acts as a thermal and salinity sink. A bronze pump with a Reeves variable speed pulley then issues the fluid through an induction type flow meter. The packing gland on the pump is adjusted so that no air may enter. From the flow meter the fluid passes through a full flow, bronze, five micron filter and thence to the settling tank at the channel's mouth. In the settling tank the fluid passes through a large mesh, a large honeycomb, a contraction section, and finally through a small honeycomb to the channel's beginning. The details of the apparatus are shown in figure 1. The flow was stratified by placing five salt injectors fourteen feet downstream from the channel entrance. At this point, the ratio of distance from the entrance to depth was 100. The flow was fully developed turbulence -- the finite amplitude question. The test section was five feet downstream from the injectors where their wake had dissipated and the flow had returned to steady state conditions for the neutral case. The test section was six feet upstream from the dam to avoid any end effects, such as internal hydraulic jumps.

The saturated salt water injection rate was regulated by the control tank. In the control tank a float attached to a lever operated a mercury level switch which opened and closed a valve from a storage tank of 445 gallons capacity. The depth of water in the control tank was regulated to $\pm$ 0.25 inches. The constancy of the injection flow rate is shown in figure 3. The injectors were placed at a normalized distance from the bottom of the channel of $z/h = .79$. The injection flow rate was 6cm./sec. and the jets lost their definition after 8cms. from the injectors.

b) Density Measuring Techniques

The density profiles were measured by taking samples of the fluid at various depths and feeding them into a precision hydrometer. The density probe had a horizontal dimension of 0.2 inches, and a vertical dimension of 0.035 inches, and traversed the flow on a vernier carriage. The hydrometer was a Brooks Instrument continuously reading type where the liquid flowed in through a needle valve at the bottom and out through two discharge tubes inside the glass cylinder. The hydrometer was calibrated by measuring the density of fresh water at several different temperatures and comparing the results with the data from the Handbook of Chemistry and Physics. The resolution was $\pm$ .0003 gm./cc. This instrument is shown in figures 4 and a discussion of its use is presented in section four.

c) Velocity Measuring Techniques

The measurement of the velocity, a fluctuating vector, in a varying density field is a considerably more difficult proposition, and a great deal of time went into developing this instrumentation. A pitot tube was used in the conventional manner for calibration and for mean velocity profiles in the neutral case. It proved useless in the stratified case as figure 6 indicates. The theory of a pitot tube requires that the fluid decelerate isentropically to the stagnation point. Considering a turbulent flow, we

integrate the momentum equation along the center stream line from the point where the velocity is that of the flow to the stagnation point where the velocity is zero (about four diameters of the tube, Goldstein, 1965).

1.) $U^* \frac{\partial U^*}{\partial x^*} + \frac{1}{\rho} \frac{\partial P^*}{\partial x^*} = -\frac{\partial}{\partial z} \overline{u'w'} - \frac{\partial}{\partial x^*} \overline{u'^2}$ along the streamline

Now let: $x^* = x_0 x$, $z = \alpha x^* = \alpha x_0 x$

where $\alpha \approx \frac{1}{4}$

and $U^* = U_0 U$, $\frac{1}{\rho} \frac{\partial P^*}{\partial x^*} = \frac{U_0^2}{x_0} \frac{\partial P}{\partial x}$

where U_0 is the velocity of the flow at that point.

Then, equation 1.) becomes:

2.) $\frac{1}{2} \frac{U_0^2}{x_0} \frac{\partial U^2}{\partial x} + \frac{U_0^2}{x} \frac{\partial P}{\partial x} = \frac{1}{\alpha x_0} \frac{\partial \overline{u'w'}}{\partial x} - \frac{1}{x_0} \frac{\partial \overline{u'^2}}{\partial x}$

Rearranging:

3.) $\frac{1}{2} \frac{\partial U^2}{\partial x} + \frac{\partial P}{\partial x} = -\frac{1}{\alpha} \frac{\partial \overline{u'w'}/U_0^2}{\partial x} - \frac{\partial \overline{u'^2}/U_0^2}{\partial x}$

Now, as $\frac{\overline{u'w'}}{U_0^2} < \frac{\overline{w'^2}}{U_0^2} << 1$ over most of the flow,

then:

4.) $\frac{1}{2} \frac{\partial U^2}{\partial x} + \frac{\partial P}{\partial x} = 0$

and

5.) $\frac{1}{2} U^{*2} = \frac{1}{\rho} (P_{stagnation} - P_{static})$

The pitot tube can be used in a neutral turbulent flow for mean velocity profiles and calibration.

In as much as we want to measure turbulent velocities in a stratified field, we need an instrument that has a high resolution in space and time and is not effected by a varying density field. This is the hot film

anemometer. Hot wires have been used successfully for years in air born turbulence. In going from air to water born turbulence five major problems are encountered which have only recently been solved. Even then hot films are tempermental in a liquid, particularly a salty one. Dirt in the water building up on the hot film, ground loops creating leakage from the hot film through the conducting fluid to the channel supports, air bubbles coming out of solution and attaching to the film, and deterioration of the insulating quartz film and hydrolizing of the platinum heating element are initially encountered. Also, the low over heat ratio necessary to minimize the air bubble problem causes the film to be a good thermometer. Small temperature changes of the fluid ($\sim 1^{o}C$) cause a large change in the calibration curve. To cope with these problems a full flow, five micron filter was installed in the recirculating line and the channel was covered with a polyethylene sheet. This completely eliminated the dirt problem. The channel was made of 1/2 inch plastic and the supports were wooden, thus eliminating the ground loop problem. The 2000 gallon underground sump allowed the water to come to equilibrium in regards to dissolved air and minimized the air bubble problem. With the above conditions the life time of the films was usually about seven hours in salt water, sufficient time to complete a run. In fresh water the life time was much longer. The films exhibited a shelf life after having been used in salt water. The 2000 gallon sump was a thermal sink and kept the temperature of the fluid constant, usually to better than 0.1°C during the running time of three hours for the velocity measurements. This caused no drift in calibration.

The hot film is shown in figure 5 and the electronics in figure 2. The hot film traversed the center cross-section on a vernier carriage. In the region near the wall where there are strong gradients an ocular micrometer was used to determine the distance from the wall. The instrument was aimed at a shallow angle to the channel bottom and the distance between the hot film and

its reflection in the bottom was measured. The micrometer read to .0001 inch and the resolution of the distance was .0005 inch. The hot film and its electronics are Thermo-Systems equipment of the constant temperature variety, reducing the non-linear problem in the region of large fluctuations. For a fluctuating to mean velocity ratio of .20 the fluctuating velocity error is only a few per cent (Hinze, 1959). The hot film and electronics response is flat out to 5 KHz, well beyond the spectral range of water born turbulence. The hot film is made by drawing a quartz rod to one, two or six mils. The one and two mil rods were used in the neutral case; whereas, the six mil was used in the stratified case beacuse of its better durability. An 80 angstrom platinum covering is sputtered on the center region of the quartz rod and gold is sputtered on the ends to be welded to the supporting needles. The corner weld sections and the gold are covered with epoxy resin while the platinum heating surface is insulated by a few angstroms of sputtered quartz. Because of the platinum thickness to length ratio, there was no problem of end losses. The film lengths varied from 0.02 inch to 0.08 inch.

d) Calibration of the Hot Film

The heat transfer from a hot film is more complicated than from a hot wire. It is a function of many variables some of them not easily defineable. The several heat transfer theories from heated, infinite cylinders were of little help as the results did not collapse to a single curve. Because of this, empirical calibration was necessary.

Two methods were employed. First, two concentric plastic cylinders, electrically insulated from ground, were filled with the desired fluid and brought up to solid body rotation. The hot film was then inserted, and the mean voltage vs. velocity were taken, making sure that the wake did not interfere. After three rotations the wake caused a downward drift in voltage. The calibration was done for velocities from zero to 28 cm/sec and

for salt water densities from 1.000 gm./cc. to 1.116 which is greater than the range encountered in the stratified flow. The heat transfer was found to have no dependence on salinity as M. D'Allonnes, (1970) also found. It was determined that the heat transfer for a given film and a given run was,

$$Q = f(T_a, \Delta T, u) = \frac{e^2}{R_w} \text{ times a constant}$$

where e is the voltage output from the anemometer bridge and Rw is the resistance of the hot film.

If the fluid temperature, Ta, and the overheat ratio, were held constant, the heat transfer went as the square root of the velocity. The Rayleigh No. of the hot film was small and the zero velocity transfer was conductive. These results are shown in figure 7. Immediately prior to each stratified run, the hot film was calibrated in the neutral turbulent flow by a pitot tube. The ambient temperature, Ta, and overheat ratio, ΔT, were frequently checked and found to be constant for the results presented. Reproducibility of velocity was generally $\sim 0.5\%$

e.) Processing of the Data

In processing the data two criteria had to be met. The electronics had to respond to frequencies from near zero to 5 KHz. The spectrum of turbulent water occurs at lower frequencies than that of air. Also the system had to be on line, giving the resultant mean and fluctuating voltages immediately. A small drift in the hot film voltage produces a large drift in the velocity calibration curve as:

$$e^2 = e_o^2(u=0) + B\sqrt{u} \Rightarrow u \sim e^4$$

where e_o^2 is a constant times the zero velocity heat transfer, and B is the slope of the calibration curve. This drift could be picked up immediately by observing the mean voltage output. Small air bubbles attached to the film produce a large postive change in the rms of the fluctuating voltage. Because of these requirements, a tie in with an EAI analog computer two building away was installed. A closed circuit television link was also installed to observe

the operation of the computer and, in particular, the mean voltage off of a four place digital voltmeter on the computer. An audio link allowed the immediate observation of computer malfunction via the overload alarm, as well as the beginning of each integration period. A one minute integration time was sufficient to include the low frequency energy in the rms fluctuation output. As a result of the visual and audio links, the computer was made a slave station to the laboratory.

In the first eight months of operation the Beldon shielded cable was adequate to avoid any noise pick-up between the laboratory and the computer. This changed abruptly, and the signal to noise ratio became less than one. After much effort to locate the source, it was decided to build a common mode rejection device at the computer. This eliminated the noise to less than one millivolt, quite adequate for our purposes. The system was checked by introducing a known DC voltage and sine wave into the transmission line at the laboratory station. For frequencies from .01 Hz to 5 KHz and amplitudes from .01 volts to 0.5 volts, the computer output was exact to within the ability to measure the input. This input more than encompassed the range found in water born turbulence. The schematic is shown in figure 2.

The mean velocity was determined by using the calibration curve. That is:

$$U = \left(\frac{e^2 - e_o^2}{B}\right)^2$$

The fluctuation rms velocites were found by using the slope of the calibration curve. That is:

$$\sqrt{\overline{u'^2}} = \frac{dU}{de}\sqrt{\overline{e'^2}} \Rightarrow \sqrt{\overline{u'^2}} = \frac{4e\sqrt{\bar{U}}}{B}\sqrt{\overline{e'^2}}$$

These profiles along with the density profiles were then fed into the numerical program of the first integral of the equations of motion, which yield the momentum and mass fluxes. This is presented in detail in section four.

3. The Neutral Case

a.) Comparison of the Mean and Fluctuating Profiles with those of Air Borne Turbulence

In approaching the measurement of turbulence in a stratified flow, the investigation of water born turbulence in the neutral case was felt to be a necessary first step. This was done to reproduce the well known results from air borne turbulence, and to verify the velocity instrumentation. Ideally, isotropic, homogeneous turbulence, where there is an appeal to theory, would be the first step. However, we proceeded directly to the shear flow- the analog in water of Laufer's wind tunnel experiment. This is the initial condition for the flow which then becomes stratified. The neutral case has three parts: the structure of a fully developed, steady state, two dimensional turbulence shear flow; the requirements for two dimensionality and steady state; and the nature of the flow as the free surface is approached. This region is distinct from Laufer's central region and little is known of it.

The neutral case exhibited the expected "Law of the Wall" mean velocity distribution. That is:

$$\frac{\bar{u}}{u_*} = \frac{1}{k} \ln \frac{u_* z}{\nu} + A$$

For a Re.No. = 9,400 , figure 8, $k = .35 \pm$ and $A = 4.0 \pm .6$.
For a Re.No. - 20,000, figure 9, $k = .41 \pm .01$, and $A = 5.8 \pm .8$. Laufer, (1951) for Re. No.$\sim 10^5$ found k = .33 and A= 5.5. For large Re. No. ($\sim 10^6$) the literature generally give k = .41. There is less agreement on the value of A. Clauser, (1956), found k = .41 and A = 4.9 for Re. No. $\sim 10^6$. All of the above results are for hydraulically smooth surfaces. The logarithmic law of the wall, the local equilibrium region, extends over 60% of the depth, which is approximately what Laufer found, but well beyond the theoretical prediction and what other investigators have found in regards to turbulent boundary layers. The region where the velocity gradient is linear, the laminar sublayer, was found to extend out to where $\frac{u_* z}{\nu} \approx 5$ which was in agreement with Laufer. This region is shown in figure 10 and 11. The distribution of $\sqrt{\overline{u'^2}}$ is in agreement with Laufer as shown in figures 12 and 13. Initially a vertical probe was used causing a flow down the probe in in the region of strong shear and causing the rms results to be low (fig 12); the inclined probe shown in figure 5 removed this problem.

b.) Requirements for Two Dimensionality

The mean velocity profile is quite insensitive to deviations from two dimensionality and steady state conditions. The most sensitive quantity to deviations from two dimensionality is the normalized rms value of the velocity fluctuations, $\sqrt{\overline{u^2}}/u$. For aspect ratios (flow width to depth) less than 4.5, the normalized results did not agree with Laufer's. For aspect ratios greater they did except near the free surface. This is shown in figure 12. The stream wise development of the flow had no effect on the mean or fluctuating quantities. For a ratio of inertial terms to pressure gradient of 18% the results were unchanged.

c.) Requirements for Steady Conditions

The flow is steady state when the pressure gradient balances to Z component of the shear stress at all points in the flow. In a developing flow it was found that the effect of the inertial terms could be accurately determined by assuming a logarithmic velocity profile as shown in figure 9 over the entire cross-section. The integrated streamwise momentum equation then becomes:

6) $$\left[1 - Fr.No\frac{\partial h/\partial x - \partial h/\partial x}{\partial h/\partial x}\left\{1 - \frac{2u_s}{Hu_s} + \frac{2u^2}{R^2u_s^2}\right\}\right]\frac{1}{\rho}\frac{\partial p}{\partial x}H = -\tau_w + \tau_s \approx \tau_w$$

where Fr. No. = $\frac{u_s^2}{gH}$, $u_s = \sqrt{\tau_w}$, H = depth of the flow. Also $\frac{\partial h}{\partial x}$ is the slope of the free surface, and $\frac{\partial h}{\partial x}$ is the slope of the bottom of the channel. τ_w is the stress at the wall and τ_s is the stress at the surface (about 2% of τ_w). The term in bracket $\{\}$ is nearly constant at 0.78. Laufer found $u^2/u_s^2 = .0018$ for all Re. Nos. In this case it was .0020. The derivation of the above is carried out in Appendix I, and its validity is shown in figure 10, where the inertial terms and pressure gradient then balance the stress at the wall. The inertial terms result in an 18% imbalance between the pressure gradient and the shear. The above derivation also indicated that if the slope of the channel bottom is adjusted to equal the slope of the surface the flow will be steady state for all Fr. Nos. This was the condition for the results presented in figure 11 where the Fr. No. = .96. The pressure gradient $\frac{1}{\rho}\frac{\partial p}{\partial x} = g\frac{\partial h}{\partial x}$ was of the order of 9×10^{-3} so care had to be taken in its measurement. The pressure taps shown in figure 1 were connected to 0.5 inch glass tubes. The difference in height of the water columns was measured by a Titian Tool Supply micro measuring scope. The columns were made as large as possible and still remain

in the field of the scope and kept clean. A wetting agent was used to make the meniscus as flat as possible. The scope read to .0001 inch and the zero pressure gradient reading was reproducible to $\pm$ .0004 inch. The reproducibility of the pressure gradient (the slope of the free surface) was about 5% for Re. No. = 20,000 runs. The slope of the bottom of the channel was taken with a micro bubble gauge. This was constructed from two ten inch pieces of machined aluminum, hinged at one end and with a micrometer shaft at the other end. A precision bubble gauge was placed in the center of the top piece of aluminum. In taking a reading of the channel slope the bubble was brought to the center of the level gauge, and the micrometer reading was compared to that for zero slope. This technique was accurate to $\sim$ .0008 inch over a ten inch span. Initially, a micrometer point gauge was used to back up the surface slope measurement. All this succeeded in doing was to measure the evaporation rate. An interesting side result was that the evaporation rate varied by a factor of 20 from when the channel was covered and the water surface dirty to when it was open and the surface clean.

d.) Mean and Turbulent Properties Near a Free Surface

i.) Surface Stress and Tendency Back to Local Equilibrium

The results near the free surface differed from those of Laufer's near the center of the wind tunnel. Both the mean and fluctuating velocities increased beyond the Laufer results as the free surface was approached, as shown in figures 14 and 15. The significant difference between a free surface and the center of a wind tunnel is the appearance of a molecular film and a resultant stress at the free surface. This non zero boundary condition is usually bothersome to the laboratory experimentalist, but is of great interest to the oceanographer. The wind exerts a surface stress on the ocean currents. For a zero surface stress flow the region near the surface ($0.6 \leq z/H \leq 1.0$) is difficult to characterize because it is not in local equilibrium. Diffusion is important and the properties of this region depend upon what is happening elsewhere in the flow. As a surface stress is applied, the flow tends towards a constant stress Couette flow. The boundary condition downstream at the dam is that the Froude Number be one. This implies that the flow remains at a nearly constant depth. The velocity at the surface increases over the zero stress condition, and for a fixed flow rate, conservation

of mass requires that the velocity and shear near the wall decrease. The wall stress decreases as the surface stress increases and the flow tends towards local equilibrium where the diffusion of energy is unimportant and a balance between local energy production and dissipation occurs.

ii) Discussion of a Laminar Sublayer

The stress at the free surface was determined thusly:

7) $$\tau_s = \nu \left.\frac{\Delta U}{\Delta z}\right|_{\text{at } z/h = .99}$$

Following the same reasoning used at the bottom of the channel, the laminar sublayer is: $$\frac{\sqrt{\tau_s}\, z}{\nu} = 5$$

giving $$\frac{z}{h} = 0.93$$

The equations of motion in this region require that:

8) $$\frac{1}{\rho}\frac{dp}{dx} z = \tau_s - \tau(z)$$

and

9) $$\frac{1}{\rho}\frac{dp}{dx} h = \tau_s - \tau_w$$

thus

10) $$\nu \frac{du}{dz} = \tau(z) = -(\tau_w - \tau_s)\frac{z}{h} + \tau_w = (\tau_w - \tau_s)\left(1 - \frac{z}{h}\right) + \tau_s$$

and

11) $$U(z) = u_s - \frac{h}{2\nu}(\tau_w + \tau_s) + \frac{1}{\nu}\left[\tau_w z - (\tau_w - \tau_s)z^2/2h\right]$$

These results are plotted in figure 14 and clearly do not conform to the measured profile. This region is turbulent. The rub is that $u_{*s} = \sqrt{\tau_s}$ does not characterize the velocity here. If the surface velocity is used, then for $u_s z/\nu = 5$ the laminar sublayer occurs at $$\frac{z}{h} = .9994$$

This is considerably closer to the surface that it was able to measure and is smaller than surface disturbances. The free surface is hydraulically rough. The surface stress is larger than equation 7.) but has an upper limit from the imbalance of the corrected $\frac{1}{\rho}\frac{dp}{dx} H$ and τ_w, which is about 5% of τ_w.

iii) Theoretical Attempts to Describe the Velocity Structure

If we assume that the region near the surface is turbulent and in local equilibrium, similarity arguments can be used to predict the mean velocity structure. Prandtl, (1949), and Townsend, (1961) describe an equilibrium layer as a region where there is a balance between local turbulent energy production and dissipation, and where the macroscale of the turbulence is small compared with the scale of the change in stress. Under these conditions the formulation for equilibrium layers is:

$$\frac{dU}{dz} = \frac{\sqrt{\tau}}{\kappa z}$$

where Von Karman's constant $\kappa = .41$

For our co-ordinate system and for the free surface region this becomes:

$$\frac{dU}{dz} = \frac{\sqrt{\tau}}{\kappa h(1-z/h)}$$

where H = depth of the flow

Now $\tau(z) = (\tau_w - \tau_s)(1 - z/h) + \tau_s$

and $$\frac{dU}{dz} = \frac{\sqrt{(\tau_w - \tau_s)(1-z/h) + \tau_s}}{\kappa h(1-z/h)}$$

Integrating from z to $h-\delta$ we find:

12) $$U(z) = U(h-\delta) - \frac{2}{\kappa}\sqrt{\tau_w - \tau_s}\left[\sqrt{1 - z/h + \tau_s/\tau_w - \tau_s} - \sqrt{\delta + \tau_s/\tau_w - \tau_s}\right] - \frac{\sqrt{\tau_s}}{\kappa} \ln \frac{\left(\sqrt{1-z/h + \tau_s/\tau_w - \tau_s} - \sqrt{\frac{\tau_s}{\tau_w - \tau_s}}\right)\left(\sqrt{\delta + \frac{\tau_s}{\tau_w - \tau_s}} + \sqrt{\frac{\tau_s}{\tau_w - \tau_s}}\right)}{\left(\sqrt{1-z/h + \tau_s/\tau_w - \tau_s} + \sqrt{\frac{\tau_s}{\tau_w - \tau_s}}\right)\left(\sqrt{\delta + \frac{\tau_s}{\tau_w - \tau_s}} - \sqrt{\frac{\tau_s}{\tau_w - \tau_s}}\right)}$$

In this equation δ is the point of velocity measurement closest to the surface. The results from this equation are plotted in figures 14 and 15 for $\tau_s/\tau_w = .0016$ and $\tau_s/\tau_w = .022$. Figure 14 shows that the predicted velocity gradient is steeper than the measured. Because the diffusion of turbulent energy is probably still important for these low values of τ_s/τ_w, K_m is underestimated. Figure 15 indicates a much better agreement between theory and experiment for this higher ration of τ_s/τ_w. The agreement is good out to $(z-H)/H = .08$ where the theoretical gradient again steepens beyond the measured value.

4. Investigation of the Stratified Case

a.) Equations of Motion and Mass Transfer

The aim of this portion of the experiment is to determine the mass and momentum fluxes across the channel for various bulk Ri. Nos. and at an approximately constant Re. No. Profiles of mean density, mean velocity, and the time average of the fluctuating velocity were taken at cross sections one foot apart in the center of the channel where y=0 and $\frac{\partial}{\partial y} = 0$ from symmetry. This information along with the boundary condition, the wall shear and the

pressure gradient, was used in conjunction with the first integral of the equation of motion to determine the fluxes.

The equations of motion for an incompressible turbulent flow are:

13.) $\partial u''/\partial x + \partial w''/\partial y = 0$

14.) $\frac{\partial u''}{\partial t} + u''\frac{\partial u''}{\partial x} + w''\frac{\partial u''}{\partial z} + \frac{1}{\rho}\frac{\partial p''}{\partial x} = \nu\frac{\partial^2 u''}{\partial z^2} + \nu\frac{\partial^2 u''}{\partial x^2}$

The boussinesq approximation has been used as

$\Delta\rho/\rho \leq 0.04$ for all runs.

where $\Delta\rho$ is the difference in mean density across the flow.

15.) $\frac{\partial w''}{\partial t} + u''\frac{\partial w''}{\partial x} + w''\frac{\partial w''}{\partial z} + \frac{1}{\rho_0}\frac{\partial p''}{\partial z} = -\frac{\rho''}{\rho_0}g + \nu\frac{\partial^2 w''}{\partial z^2} + \nu\frac{\partial^2 w''}{\partial x^2}$

16.) $\frac{1}{\rho_0}\frac{\partial \rho''}{\partial t} + \frac{u''}{\rho_0}\frac{\partial \rho''}{\partial x} + \frac{w''}{\rho_0}\frac{\partial \rho''}{\partial z} = \lambda\frac{\partial^2 \rho''}{\partial z^2} + \lambda\frac{\partial^2 \rho''}{\partial x^2}$

Using the normal procedure, for a time independent mean flow, of separating the dependentvariables into a mean and fluctuating component, let:

$u'' = u + u'$, $\rho'' = \rho + \rho'$

$w'' = w + w'$, $p'' = p + p'$

By definition the integral of the fluctuating quantities over a period of time is zero. This time period, t, is found by experiment. Thus, after taking the integral over t, the equations of motion become:

17.) $\frac{\partial u}{\partial x} + \frac{\partial w}{\partial z} = 0$

18.) $\frac{\partial u'}{\partial x} + \frac{\partial w'}{\partial z} = 0$

19.) $u\frac{\partial u}{\partial x} + u'\frac{\partial u'}{\partial x} + w\frac{\partial u}{\partial z} + w'\frac{\partial u'}{\partial z} + \frac{1}{\rho}\frac{\partial p}{\partial x} = \nu\frac{\partial^2 u}{\partial z^2}$

$\nu\frac{\partial^2 u}{\partial x^2}$ is neglected, as the data from the velocity profiles of figure 16 reveals:

20.) $\frac{\Delta^2 u/\Delta x^2}{\Delta^2 u/\Delta z^2} \leq 6.2 \times 10^{-4}$

Because the stream wise scale is much greater than the vertical scale, that is from figure 16: $\frac{\Delta u/\Delta x}{\Delta u/\Delta z} = \frac{H}{L} \leq .026$

the hydrostatic form of equation (20) can be used.

We then have:

21.) $\frac{1}{\rho_0}\frac{\partial p}{\partial z} = -\rho g$

The conservaton of salinity is:

22.) $\frac{\partial \rho}{\partial t} + u\frac{\partial \rho}{\partial x} + u'\frac{\partial \rho'}{\partial x} + w\frac{\partial \rho}{\partial z} + w'\frac{\partial \rho'}{\partial z} = \lambda\frac{\partial^2 \rho}{\partial z^2}$

$-\lambda\frac{\partial^2 \rho}{\partial x^2}$ is neglected as the mean density profiles from figure 17 reveal:

$\frac{\Delta^2 \rho/\Delta x^2}{\Delta^2 \rho/\Delta z^2} \leq 3 \times 10^{-3}$

Using equation (18) and letting $\frac{1}{t}\int_0^t f(t')\,dt' = \bar{f}$

23.) $$u\frac{\partial u}{\partial x}+\frac{\partial \overline{u'^2}}{\partial x}+w\frac{\partial u}{\partial z}+\frac{1}{\rho_0}\frac{\partial p}{\partial x}=\nu\frac{\partial^2 u}{\partial z^2}-\frac{\partial \overline{u'w'}}{\partial z}$$

24.) $$\frac{\partial \rho}{\partial t}+u\frac{\partial \rho}{\partial x}+w\frac{\partial \rho}{\partial z}=\lambda\frac{\partial^2 \rho}{\partial z^2}-\frac{\partial \overline{\rho'w'}}{\partial z}-\frac{\partial \overline{\rho'u'}}{\partial x}$$

The last term in equation (24) cannot be measured with existing techniques. However, if we assume that the turbulent scales, the eddies, effecting the momentum transfer, are representative of those effecting the mass transfer and these scales go as $\overline{u'^2}$ in the stream wise direction and $\overline{u'w'}$ in the vertical, we have from figures 18 and 19 for $z/H = 0.8$

$$\frac{\overline{\rho'u'}}{\overline{\rho'w'}} \sim \frac{\overline{u'^2}}{\overline{uw}} = \frac{2.25\times10^{-1}}{1.4\times10^{-1}} = 1.6$$

and:

$$\frac{\Delta\overline{\rho'u}/\Delta x}{\Delta\overline{\rho w}/\Delta z} \sim \frac{H}{L}\frac{\overline{\rho'u'}}{\overline{\rho'w'}} = .042$$

Thus, equation (24) becomes:

25) $$\frac{\partial \rho}{\partial t}+u\frac{\partial \rho}{\partial x}+w\frac{\partial \rho}{\partial z}=\lambda\frac{\partial^2 \rho}{\partial z^2}-\frac{\partial \overline{\rho'w'}}{\partial z}$$

Next, we integrate equation (21) from zero to some value of Z and take the stream wise (x) gradient. This yields for equation (23)

(26) $$u\frac{\partial u}{\partial x}+\frac{\partial \overline{u'^2}}{\partial x}+w\frac{\partial u}{\partial z}+\frac{1}{\rho_0}\frac{\partial p_w}{\partial x}-g\frac{\partial}{\partial x}\int_0^z \rho\,dz'=\nu\frac{\partial^2 u}{\partial z^2}-\frac{\partial \overline{\rho'w'}}{\partial z}$$

Where Pw is the pressure at the wall. Integrating equation (26) from zero to Z and using equation (17) we have:

27) $$\int_0^z \frac{\partial(u^2+\overline{w'^2})}{\partial x}dz'-u\int_0^z\frac{\partial u}{\partial x}dz'+\frac{1}{\rho_0}\frac{\partial p_w}{\partial x}z-g\frac{\partial}{\partial x}\int_0^z\left[\int_0^{z'}\rho\,dz''\right]dz'+\tau_w=\nu\frac{\partial u}{\partial z}-\overline{uw'}=\tau(z)$$

where τ_w is the stress at the wall.

Now let $\int_0^{z'}\rho(z'')dz''=F(z')$ and $\frac{dF(z')}{dz'}=\rho(z'')$

then:

$$-\frac{\partial}{\partial x}\int_0^z F(z')dz'=-\frac{\partial}{\partial x}\left[F(z')z'\Big|_0^z-\int_0^z z'\frac{\partial F(z')}{dz'}dz'\right]$$

$$=-\frac{\partial}{\partial x}\left[F(z)z-\int_0^z z'\rho(z')\,dz'\right]$$

and

$$-g\frac{\partial}{\partial x}\int_0^z\left[\int_0^{z'}\rho(z'')dz''\right]=-g\frac{\partial}{\partial x}\int_0^z F(z')dz'=-gz\frac{\partial}{\partial x}\int_0^z\rho(z')dz'+g\frac{\partial}{\partial x}\int_0^z z'\rho(z')dz'$$

Equation (27) becomes:

28) $$\tau(z)=\nu\frac{\partial u}{\partial z}-\overline{uw'}=\tau_w+\frac{1}{\rho_0}\frac{\partial p_w}{\partial x}z-gz\frac{\partial}{\partial x}\int_0^z\rho(z')dz'+g\frac{\partial}{\partial x}\int_0^z z'\rho(z')dz'$$
$$+\int_0^z\frac{\partial}{\partial x}(u^2+\overline{w'^2})dz'-u\int_0^z\frac{\partial u}{\partial x}dz'$$

Equation (28) gives the distribution of the momentum flux, $\tau(z)$, as a function of the boundary conditions and the measured stream-wise gradients. Term 1 on the right hand side is the stress at the wall; Term 2 is the stream wise pressure gradient at the wall; term 3 and 4 are the contribution to the pressure gradient by the internal density gradient which will be referred to as the baroclinic pressure gradient. Term 5 is the integrated divergence of

the horizontal momentum flux and term 6 is the mean vertical momentum flux. The contribution of these terms to $\tau(z)$ for a Re. No. of 10,000 and a Ri.No. of 0.33 is presented in Table I.

Now integrating equation (25) and using equation (17):

$$29.\quad q_s(z) = \lambda_s \frac{\partial \rho}{\partial z} - \overline{\rho' w'} = \int_0^z \frac{\partial \rho}{\partial t} dz' + \int_0^z \frac{\partial}{\partial x}[\rho u] dz' - \rho \int_0^z \frac{\partial u}{\partial x} dz'$$

As the flow is recirculating, there is a slow increase in the ambient density in time. However, in the region where the salt flux is important, that is for $z/h \sim .25$, figures 20 and 21 reveal:

$$\frac{\int_0^{.4} \partial s/\partial t \, dz}{q_s(.4)} = .004$$

Also, as is shown in Table II:

$$\frac{\lambda \Delta \rho / \Delta z}{-\overline{\rho' w'}} \leq .01$$

Thus, equation (29) becomes:

$$(30)\qquad q_s(z) = -\overline{\rho' w'} = \int_0^z \frac{\partial}{\partial x}[\rho u] dz' - \rho(z) \int_0^z \frac{\partial u}{\partial x} dz'$$

Equation (30) gives the distribution of the turbulent salt flux, $q_s(z)$, across the flow as a function of the measured stream wise gradients. Term 1 on the right hand side is the integrated mean horizontal flux divergence and 2 is the mean vertical flux. The contribution of these terms to $q_s(z)$ for a Re. No. of 10,000 and a Ri. No. of 0.33 is presented in Table I.

If we let:

$$-\overline{u'w'} = K_m \frac{\partial u}{\partial z} \quad , \quad -\overline{\rho' w'} = K_s \frac{\partial \rho}{\partial z}$$

and transform equation (28) and (30) to numerical form, we then have:

$$31)\quad \tau(z) = (\nu + K_m) \frac{\Delta u(x_i, z_n)}{\Delta z_n} = \tau_w + \frac{z_n}{2} \frac{\Delta p_w}{\Delta x} - z_n g \sum_{z_i=1}^{z_i=n} \frac{\Delta \rho(x_i, z_i)}{\Delta x} \Delta z_i + g \sum_{z_i=1}^{z_i=n} z_i \frac{\Delta \rho(x_i, z_i)}{\Delta x} \Delta z_i + \sum_{z_i=1}^{z_i=n} \left[\frac{\Delta v^2(x_i, z_i)}{\Delta x} + \frac{\Delta \overline{uv}(x_i, z_i)}{\Delta z} \right] \Delta z_i - u \sum \frac{\Delta u}{\Delta x} \Delta z_i$$

$$32)\quad q_s(z_n) = K_s \frac{\Delta \rho(x_i, z_n)}{\Delta z_n} = \sum_{z_i=1}^{z_i=n} \frac{\Delta \rho(x_i, z_i) \Delta u(x_i, z_i)}{\Delta x} \Delta z_i - \rho(z) \sum_{z_i=1}^{z_i=n} \frac{\Delta u(x_i, z_i)}{\Delta x} \Delta z_i$$

The fluxes were then determined by using the raw data from the measured profiles and programing equations (31) and (32) for a digital computer. The Richardson Number:

$$\text{Ri. No.} = -\frac{g \Delta \rho / \Delta z_n}{(\Delta u / \Delta z_n)^2}$$

was determined in the same manner. The program also yielded Ks and Km by dividing the fluxes by the measured vertical gradients.

Because of the scatter in $\overline{u'^2}$ as shown in figure 18, its stream

wise gradient was neglected. However, as figures 16 and 18 indicate for $\mathcal{L}/H=0.17$

$$\frac{\Delta\overline{u'^2}/\Delta x}{\Delta U^2/\Delta x} = .02$$

It was generally much smaller than this.

Also, the scatter in measuring the pressure gradient was $\sim$ 50% (about five times poorer than in the neutral case). Consequently, the pressure gradient was adjusted to provide zero stress at the free surface.
The pressure gradient was a significant term in the momentum flux equation as indicated in Table I. As a result, large scatter in the pressure gradient created large scatter in the resultant momentum flux.

b.) The Measured Profiles

i.) Gross Features of the Developing Flow

Runs were made at a Re.No. of $\sim$ 10,000 and Ri.Nos. of 0.22, 0.30, 0.33, 0.36, and 0.38. The Re. No. was defined by using the maximum velocity and the depth of the flow. The bulk Ri. No. was defined by using the maximum velocity, the depth of the flow, and the density difference between the top and bottom of the flow.

The earlier runs made at Ri. Nos. of 0.22, and 0.33 had considerable scatter in regards to the density profiles. Consequently, the data was not reduced and the bulk Ri. Nos. must be considered approximate. The mean and fluctuating velocity profiles are useful and are presented in Appendix II.

The measured profiles presented in the graphs at the end of this section and in Appendix II indicated that for a given run over most of the cross section the mean flow is accelerating and $\overline{w^2}$, the wall stress and the bulk Ri. No. are decreasing in x. If the channel were long enough, the flow would return to the neutral case and the classical turbulent flow presented in figures 22 to 23. At some point, the possible critical Ri. No., the streamwise gradients of $\overline{u^2}$ and $\overline{u'w'}$ must become positive to return to the neutral conditions.

In going from one run to another of lower bulk Ri. No. the opposite occurs. The wall stress increases, the maximum velocity decreases. The flow is tending back towards neutral conditions.

ii) The mean Velocity Results

The mean velocity results were of high quality, reproducibility in general being better than one percent as indicated in figures 16, II-1 and II - 3. More than twice as many runs were made than are presented here. Initially a pitot tube was used to make a survey over a wide range of Ri. Nos. to

determine what range to use the more detailed hot film instrumentation. The pitot tube proved to be useless in the stratified case as the scatter shown in figure 6 indicates. The hot films were not of uniform quality and had a shelf life, particularly after having been used once in saline water. Sometimes they would deteriorate abruptly as was the case in the third cross section of figure II-1. Other times they would exhibit a slow drift. As the mean velocity goes as the fourth power of the measured voltage, an on-line system with a very accurate voltmeter is necessary to continuously monitor the equipment performance. A closed circuit television system read the voltage output directly off of the four place digital voltmeter on the computer. When the hot films worked, they worked quite well.

iii) The fluctuating Velocity Results

The rms of the voltage fluctuations was also continuously monitored. The results of the run shown in figure II-2 are presented even though a significant change in the calibration of the hot film occurred. The rms fluctuations depend upon the slope of the calibration curve and are less affected by a displacement of it.

Another reason for the on-line system was to immediately detect and reject the rms results that were affected by air bubbles forming on the hot film. The rms of the fluctuating voltage would in general show an immediate change when this occurred. Air bubbles coming out of solution and adhering to the back of the hot film caused virtually no problem in the neutral fresh water runs when the water was sufficiently aged. However, in the stratified case, particularly in the interior regions where strong mixing occurred, this was a problem. The dissolving of salt into fresh water lowers its saturation level and makes air bubbles more prone to come out of solution. Small bubbles would reduce the mean heat transfer, a large bubble would increase it, and sometimes two large bubbles close to each other would reduce it. All bubbles seemed to increase the fluctuating component. The scatter in the rms of the velocity fluctuations seemed to come from bursts of energy. Intermitancy is a problem found by many other investigators. There is also the possibility that small bubbles , formed towards the end of the integration period, went undetected and had some effect. The mean conditions remained constant as monitored by the flow meter, the depth and temperature of the flow, and the reproducibility of the mean velocity. Also the salt water injection rate proved to be quite constant.

An interesting qualitative observation in regards to the fluctuations, is that in the region where they are largest, internal waves were visually observed.

iv) The Density Profiles

Considerably more difficulty developed in measuring the mean density profiles. The problems were not wholly resolved until the last run, represented in figures 16 to 33; consequently the previous runs should be viewed qualitatively. Because the flow is recirculating, there is an increase in the ambient density of the flow upstream of the salt injectors. This rate of increase is negligible in the equations of motion as was previously shown, but must be taken into account in correcting the measured density profiles. The mean conditions of the flow remained constant, as did the injection flow rate of salt water shown in figure 3; however, the rate of increase of the ambient density exhibited considerable scatter until the last run. Initially, the ambient density was monitored by placing the density probe near the surface and downstream of the test section during the three hours the velocity profiles were taken. This was found to indicate a much higher rate of ambient density increase than was true. The wake of the velocity probe caused this anomaly. In the last run the density near the surface was monitored in the test section when the density profiles were taken. The results are shown clearly in figure 20.

Another possible source of error that was corrected in the last run, figures 16 to 33, was the possible mixing of fluid from one data point when the next data point was taken. Rather than use the hydrometer as a continuously reading instrument as it was designed for, it was emptied after each data point and slowly filled at the next one.

In using the density probe ideally the velocity of fluid entering the probe should match or be less than that of the flow at that point. In the last run the maximum possible filling time of the hydrometer of four minutes was used. This limit is imposed because of the storage capacity of saturated salt water and the time required to take all of the data which was about six hours. The probe entry velocity for a four minute filling time was 42 cm/sec. In an unstratified flow the probe's resolution at an approach velocity of 18 cm/sec was observed by the use of dye streaks. The resolution was essentially that of the probe's dimension of .089 cm. This technique was not able to be used in the low velocity, strong gradient region near the wall in the stratified case, because of the fluctuating density and index of refraction.

This is a source of possible systematic error in the density profiles. It would affect the vertical gradients near the wall, but should have little effect on the streamwise gradients as the velocity, the density and their vertical gradients are similar at each cross section.

c.) The Results of the First Integral of the Equations of Motion

i.) The Momentum and Mass Fluxes

Initially, to determine the momentum and mass fluxes, three cross sections were taken. These mean and fluctuating profiles are shown in Appendix II. This was reduced to a two cross section run so that more time would be allowed for individual measurements, particularly in regard to the density profiles. The numerical program for equations (31), (32) was worked out manually in its entirety for six of the 16 values of n in the case of the mass transfer, and for two values of n in the momentum case. Also several of the individual terms in the momentum equation for larger values of n were checked, and the first term in the mass transfer equation was worked out for all values of n.

The error bars were determined by introducting in the computer program an error of 2 1/2% in the velocity (an error of 12% in the streamwise gradient) at the lowest value of n where large changes occur; that is for n=4 and Z/h=.062. This error is considerably larger than the measurement errors at the two adjacent points that determine the vertical gradient. However, because the velocity used to determine the streamwise gradient had to be read from the curve drawn connecting the two adjacent points, the uncertainty in curvature at this value of n might produce this magnitude of error. Similar errors in velocity were introduced at larger values of n. They produced much smaller error bars. Errors in density are not included as they also have a much smaller effect. The inertial terms dominate as Table I indicates and the percentage error in the streamwise density gradient is smaller. The error bars in the mass transport, q_s, are larger as two relatively large terms that are nearly equal are subtracted from one another. This is pointed out in Table I and Figure 24.

A strong indicator of the reliability of the salinity flux results is the conservation of mass at the two cross sections, that is:

$$\frac{\int_0^{h_2} \rho(x_2, z)\, u(x_2, z)\, dz}{\int_0^{h_1} \rho(x_1, z)\, u(x_1, z)\, dz}$$

The difference between these is the first term in the mass flux equation and should be nearly zero at the surface. In the last run, figures 16 to 33, these terms were within 0.08% of each other. In the previous runs they were from 1% to 4% of each other. The preceeding error analysis is not intended to give the absolute error bars, but rather to give an indication of what they are.

ii) Energy Budget for a Developing Flow

Considering the momentum flux, and particularly that component produced by turbulence, $\overline{u'w'}$, of figures 19 and 26, the most striking features is that it is negative over the lower portion of the flow. At this point, it is useful to remember that in a turbulent system we have a balance between the mean advection and pressure gradient and the fluctuating inertial terms which sometimes act as dissipative terms. It is clear from the results of $\overline{w'^2}$ and $\frac{\Delta U}{\Delta x}$ that if we define

$$-\overline{w'^2} = K_{mx}\frac{\Delta U}{\Delta x}$$

then, for the upper portion of the flow where

$$\Delta U/\Delta x > 0$$

then,

$$K_{mx} < 0$$

In regard to $\overline{u'w'}$ the turbulent energy budget equation should be reconsidered in light of the developing aspect of the flow. In general from Phillips, (1966), this is:

$$(33)\quad \frac{1}{2}\frac{D\overline{u_i'^2}}{Dt} + \frac{\partial}{\partial x_j}\left[\overline{u_j'\left(\frac{u_i'^2}{2} + \frac{p'}{\rho}\right)}\right] = -\overline{u_i' u_j'}\frac{\partial U_i}{\partial x_j} - g\overline{\rho' w'} - \phi$$

Where ϕ is viscous dissipation and is positive. For a two dimensional developing flow this becomes:

$$(34)\quad -\overline{u'w'}\frac{\partial U}{\partial z} - g\overline{\rho' w'} - \phi = U\frac{\partial}{\partial x}\frac{\overline{u'^2}+\overline{v'^2}+\overline{w'^2}}{2} + W\frac{\partial}{\partial z}\frac{\overline{u'^2}+\overline{v'^2}+\overline{w'^2}}{2} + \overline{w'^2}\frac{\partial W}{\partial z}$$
$$+\overline{u'w'}\frac{\partial W}{\partial x} + \frac{\partial}{\partial x}\left[\overline{u'\left(\frac{u'^2+v'^2+w'^2}{2} + \frac{p'}{\rho}\right)}\right] + \frac{\partial}{\partial z}\left[\overline{w'\left(\frac{u'^2+v'^2+w'^2}{2} + \frac{p'}{\rho}\right)}\right] + \overline{w'^2}\frac{\partial U}{\partial x}$$

if we let:

$$-\overline{u'w'} = K_{mz}\frac{\partial U}{\partial z}\quad , -\overline{u'^2} = K_{mx}\frac{\partial U}{\partial x}$$

$$-\overline{w'^2} = K_{mz}\frac{\partial W}{\partial z}\quad , -\overline{\rho' w'} = K_s\frac{\partial \rho}{\partial z}$$

we then have:

$$(35)\quad \left[1 + \frac{gK_s\,\partial\rho/\partial z}{K_{mz}(\partial U/\partial z)^2} - \frac{\phi}{K_{mz}(\partial U/\partial z)^2}\right] = \frac{U\frac{\partial}{\partial x}\left(\frac{\overline{u'^2}+\overline{v'^2}+\overline{w'^2}}{2}\right)}{K_{mz}(\partial U/\partial z)^2}$$

$$+\frac{W\frac{\partial}{\partial z}\left(\frac{\overline{u'^2}+\overline{v'^2}+\overline{w'^2}}{2}\right)}{K_{mz}(\partial U/\partial z)^2}+\frac{\frac{\partial}{\partial z}\left[\overline{u'\left(\frac{u'^2+v'^2+w'^2}{2}+\frac{p'}{\rho}\right)}\right]}{K_{mz}(\partial U/\partial z)^2}$$

$$+\frac{\frac{\partial}{\partial z}\left[\overline{w'\left(\frac{u'^2+v'^2+w'^2}{2}+\frac{p'}{\rho}\right)}\right]}{K_{mz}(\partial U/\partial z)^2}-\frac{K_{mx}\left(\frac{\partial U}{\partial x}\right)^2}{K_{mz}\left(\frac{\partial U}{\partial z}\right)^2}-\frac{\frac{\partial W}{\partial x}}{\frac{\partial U}{\partial z}}-\frac{\left(\frac{\partial W}{\partial z}\right)^2}{\left(\frac{\partial U}{\partial z}\right)^2}$$

where

$$\frac{g K_s \partial\rho/\partial z}{K_{mz}(\partial U/\partial z)^2} = -R_{f.\,No.}$$

In the steady state case the right hand side of equation (35) is zero, limiting the Rf. No. to less than one. In our case the first two terms on the right represent the advection of turbulent energy. The third and fourth terms represent the vertical and streamwise diffusion of turbulent energy. The physical meaning of the remaining terms is not clear. Thus, in a developing flow the Rf.No. can be greater than one and turbulence still persist if the vertical and streamwise gradients of the turbulent fluctutations are negative. To say this another way the Rf. No., as defined, does not properly assess the kinetic energy available for mixing. Rearranging equation (35) we have:

(36)
$$-\overline{u'w'} = K_{mz}\frac{\partial U}{\partial z} = \frac{-gK_s\,\partial\rho/\partial z}{\partial U/\partial z\left[1+\frac{\partial W/\partial z}{\partial U/\partial x}+\frac{(\partial W/\partial z)^2}{(\partial U/\partial z)^2}\right]}$$

$$+\frac{\Phi}{\partial U/\partial z\left[1+\frac{\partial W/\partial z}{\partial U/\partial x}+\frac{(\partial W/\partial z)^2}{(\partial U/\partial z)^2}\right]}+\frac{\frac{1}{2}U\,\partial/\partial x\left(\overline{u'^2}+\overline{v'^2}+\overline{w'^2}\right)}{\partial U/\partial z\left[1+\frac{\partial W/\partial z}{\partial U/\partial x}+\frac{(\partial W/\partial z)^2}{(\partial U/\partial z)^2}\right]}$$

$$+\frac{\frac{1}{2}W\,\partial/\partial z\left(\overline{u'^2}+\overline{v'^2}+\overline{w'^2}\right)}{\partial U/\partial z\left[1+\frac{\partial W/\partial z}{\partial U/\partial x}+\frac{(\partial W/\partial z)^2}{(\partial U/\partial z)^2}\right]}+\frac{\partial/\partial x\left[\overline{u'\left(\frac{u'^2+w'^2+v'^2}{2}+p'/\rho\right)}\right]}{\partial U/\partial z\left[1+\frac{\partial W/\partial z}{\partial U/\partial x}+\frac{(\partial W/\partial z)^2}{(\partial U/\partial z)^2}\right]}$$

$$+\frac{\partial/\partial z\left[\overline{w'\left(\frac{u'^2+v'^2+w'^2}{2}+p'/\rho\right)}\right]}{\partial U/\partial z\left[1+\frac{\partial W/\partial z}{\partial U/\partial x}+\frac{(\partial W/\partial z)^2}{(\partial U/\partial z)^2}\right]}-\frac{K_{mx}(\partial U/\partial x)^2}{\partial U/\partial z\left[1+\frac{\partial W/\partial z}{\partial U/\partial x}+\frac{(\partial W/\partial z)^2}{(\partial U/\partial x)^2}\right]}$$

In equation (36) the Reynolds stress, the term on the left, is balanced by the bouyancy and viscous forces, the first two terms on the right, as well as the intertial forces of turbulent advection and diffusion, the third, fourth, fifth and sixth terms on the right. The physical meaning of the last term is not clear. Thus, $K_{mz}\frac{\partial U}{\partial z}$ and K_{mz} (as $\partial U/\partial z$ is always positive) can be negative if the vertical and streamwise gradients of the turbulent fluctuations are strongly negative.

The implications of equation (36) can be seen in the results presented in figures 19 and 27. The Reynolds stress, $-\overline{u'w'}$, and the Austausch coefficient, K_{mz}, are negative in the region near the wall. One of

the terms on the right hand side of equation (22) can be approximately determined from the measured profiles. For z/h =.20 of figures 18 and 19 we have:

$$\overline{u'w'}(.20) = -.066 \text{ cm}^2/\text{sec}^2$$

and

$$\frac{U \frac{\partial \overline{u'^2}/2}{\partial z}}{\partial U/\partial z} = -.01 \text{ cm}^2/\text{sec}^2$$

The downstream station four results should be considered more reliable as the streamwise gradients used to determine them more properly apply here. The implications of equation (35) can be seen in the upper region of the flow. The flow is highly turbulent (Km_z is $\sim$ 15 times that of the viscosity as shown in figure 27) and the Ri. No. is of order three. The Rf. No. involves the ratio of ks/kmz and is possibly smaller than the Ri. No. Unfortunately, Ks is not presented for this region as both the flux and the gradients approach zero, making Ks indeterminate. However, because this region is quite turbulent, Ks would be similar to Kmz and the Rf. No. would be close to the value of the Ri. No.

iii.) Austausch Coefficients and the Local Richardson Number

Figure 28 shows the momentum and salinity coefficients as a function of the local Ri. No. for the upstream and downstream cross sections of the last run. The momentum coefficient shows considerable scatter and does not show the expected reciprocal relationship to the local Ri. No. as it is defined. It is not a single valued function of the local Ri. No. This is thought to be the result of the importance of advection in the momentum balance in the different regions of the flow. This will be discussed in more detail in the next section. The salinity coefficient behaves in the expected manner with the coefficient decreasing as the local Ri. No. increases with the exception of the region near the wall. In going from near zero to a Ri. No. of 3.25 the coefficient decreases by a factor of five, although it is still some 200 times its molecular value. For a Ri. No. of 3.25 the slope of the curve is still significant. This indicates that a much larger local Ri. No. is necessary to determine a possible asymototic value.

iv.) Regimes of the Flow

By considering the various terms that contribute to the momentum flux as a function of depth three regimes of the flow can be established. In figure 29 the mean advective fluxes and their sum are plotted. Taken individually they are mathematical book keeping. It is their sum which has physical meaning and is plotted in figure 30 to determine the regimes of the flow. For $z/h < .35$ the Reynolds stress is negative and is balanced by the sum of the mean advective fluxes. The momentum Austausch coefficient is negative and of the order of the molecular viscosity as shown in figure 31. Also from figure 16

the streamwise mean velocity gradient is negative. Figure 18 shows that the streamwise fluctuating velocity, $\overline{w'^2}$, has a greater negative gradient here than in the rest of the flow. This, considering the energy budget equations is consistent with $K_m \frac{\partial U}{\partial z}$ being negative. At z/H = .35, the curves of $\overline{w'^2}$ at station two and station four intersect and the gradient is zero. Another feature of this region is that the vertical mean velocity gradient with the exception of very close to the wall is increasing in a stream wise direction. This is consistent with u' and w' being greater than zero or both being less than zero. Figure 16 shows that the mean velocity profiles intersect at z/H = .30 and above this point the flow is accelerating. This along with the fact that internal gravity waves are observed in the lower regime of the flow suggests that the critical layer mechanism is transferring momentum from the fluctuations to the mean flow. Bretherton (1967, 1969) points out that, if the local Ri. No. is greater than 0.25, internal gravity waves are attenuated by a factor $\exp\{-2(Ri.No - 0.25)^{1/2}\}$ and their momentum is transferred to the mean flow. Figures 32 and 33 indicate that the local Ri. No. is approximately 0.25 at the point where the flow begins accelerating. For .35<z/H<.85 the Reynold stress is large and positive and is balanced by the baroclinic pressure gradient. That is:

$$-\overline{u'w'} \sim \int_0^z \left[\int_\bullet^{z'} \frac{\Delta \rho}{\Delta x} \Delta z'' \right] \Delta z'$$

The momentum Austausch coefficient is large and positive as is the local Ri.No. For the surface region, Z/h > .85, the Reynolds stress, the Austausch coefficient, and the local Ri. No. all tend to zero.

The salinity flux across the flow exhibits three regimes also, although they are not coincidental with the momentum case. Figure 24 shows the mean advective fluxes that contribute to the turbulent salinity flux. They are both large compared to the turbulent component and are of opposite sign. For the wall region Z/h < .06, Figure 28 shows that the salinity Austausch coefficient is small and increasing, although two orders of magnitude greater than the molecular value. The Ri. No. is also small and increasing. For the central Region, .06 < Z/h < 0.6, the Austausch coefficient is large and exhibits the expected reciprocal relationship to the local Ri. No. Also shown in Figure 28 is the empirical relationship $\frac{K_s}{K_{s0}} = (1 + \sigma Ri)^{-1/2}$ where K_{s0} is the value for near neutral conditions. This relationship has been used with σ=8 by several investigators to model the thermocline and shows a rather poor fit to the data. A curve with σ adjusted to six to fit the data at Ri. No. = 3.0

does not fare much better. The slope of the data at Ri. = 3.25 is still significant and is larger than the two above mentioned empirical recipes. For this reason is did not seem worthwhile to develop an empirical formula for k_s at large Ri. Nos. And finally, for $Z/h > .6$, the flux and the density gradient go to zero, making the Austausch coefficient indeterminate.

I would like to thank Professor Allan R. Robinson of Harvard University who first suggested to me the importance of stratified turbulence to oceanic processes. His guidance and comments were invaluable. This work was supported by the Office of Naval Research under contract no. N-00014-67IA-0298-0011.

BIBLIOGRAPHY

Bretherton, F. (1969), "On the Mean Motion Induced by Internal Gravity Waves," Journal of Fluid Mechanics, 36, p. 50.

Bretherton, F. (1967), "The Critical Layer for Internal Gravity Waves in a Shear Flow," Journal of Fluid Mechanics, 27, p. 33.

Clauser, F. H., (1956), "The Turbulent Boundary Layer," Advances in Applied Mechanics, 4, 1-51.

Ellison, J. H. and Turner, J. S. (1960), Journal of Fluid Mechanics, 8, 514-544.

Goldstein, S., (1965), Modern Developments in Fluid Mechanics, Vol. II.

Hinze, J. (1959), Turbulence, McGraw-Hill, p. 119.

Laufer, J. (1951), NACA Report 1053, pp. 1247.

Phillips, O. M., (1966), The Dynamics of the Upper Ocean, Cambridge University Press, p. 200.

Prandtl, L., (1949), The Essentials of Fluid Dynamics, Hafner Publishing Co,, p. 125.

Revault d'Allonnes, M. (1970), Doctoral Thesis, La Faculte des Sciences de Paris.

Townsend, A., (1961), Journal of Fluid Mechanics, 11, p. 97.

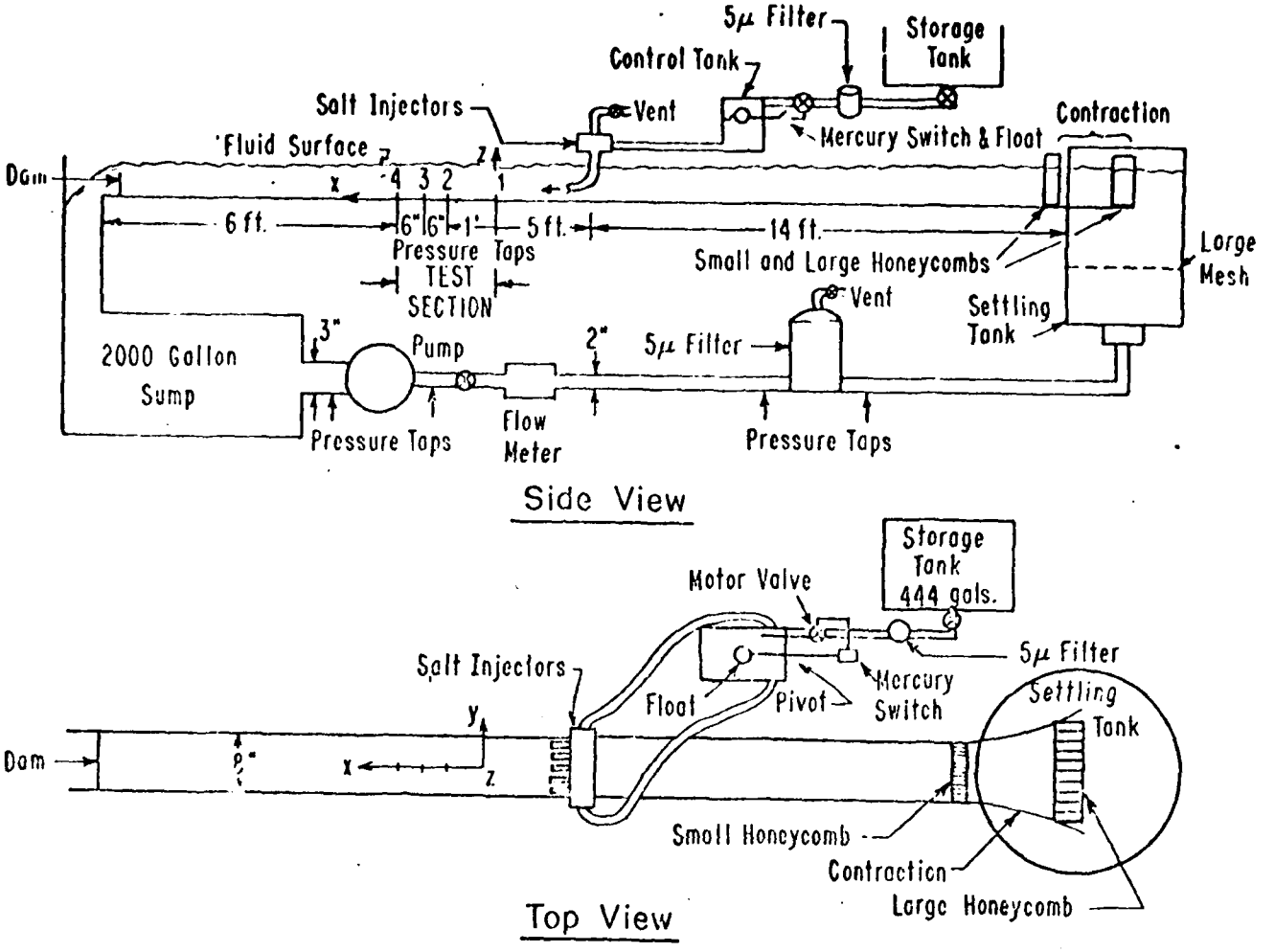

FIG. 1 WATER - FLUME

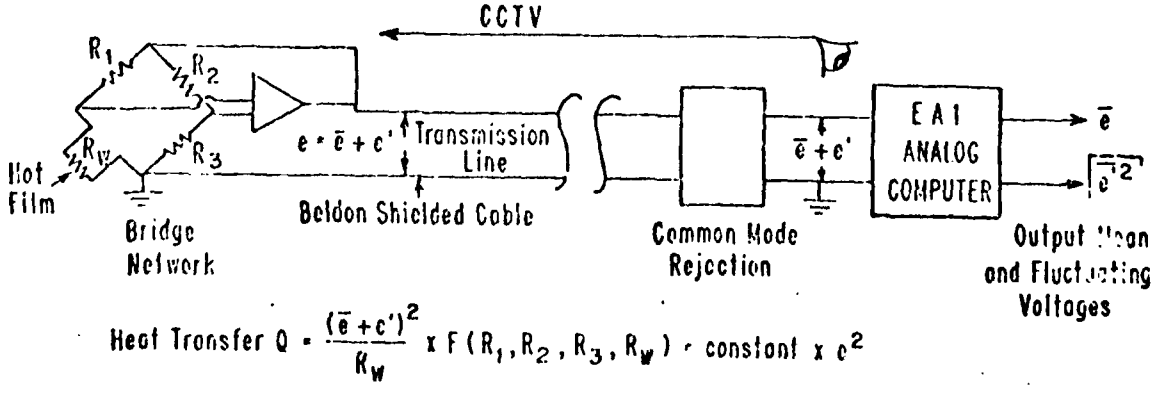

Heat Transfer $Q = \frac{(\bar{e}+e')^2}{R_w} \times F(R_1, R_2, R_3, R_w) = \text{constant} \times e^2$

FIG. 2 HOT FILM ELECTRONICS

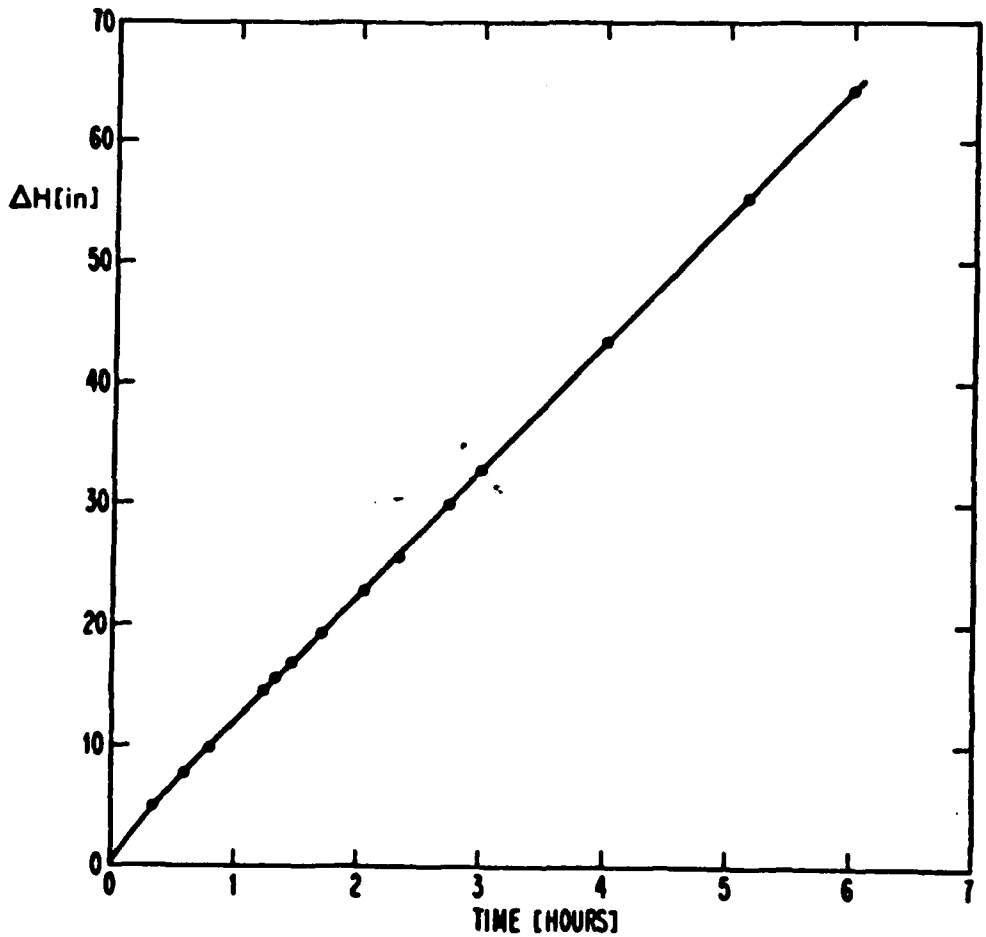

FIG. 3 SALT WATER INJECTION FLOW RATE. ΔH = DECREASE IN THE DEPTH OF THE SALT WATER TANKS. $\Delta H/\Delta t$ = .174 in/min. = 1.16 gpm.

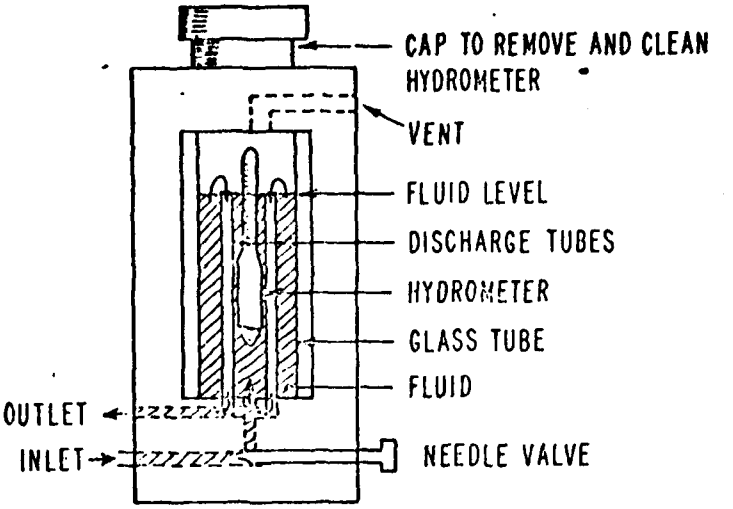

FIG. 4 CONTINUOUSLY READING HYDROMETER

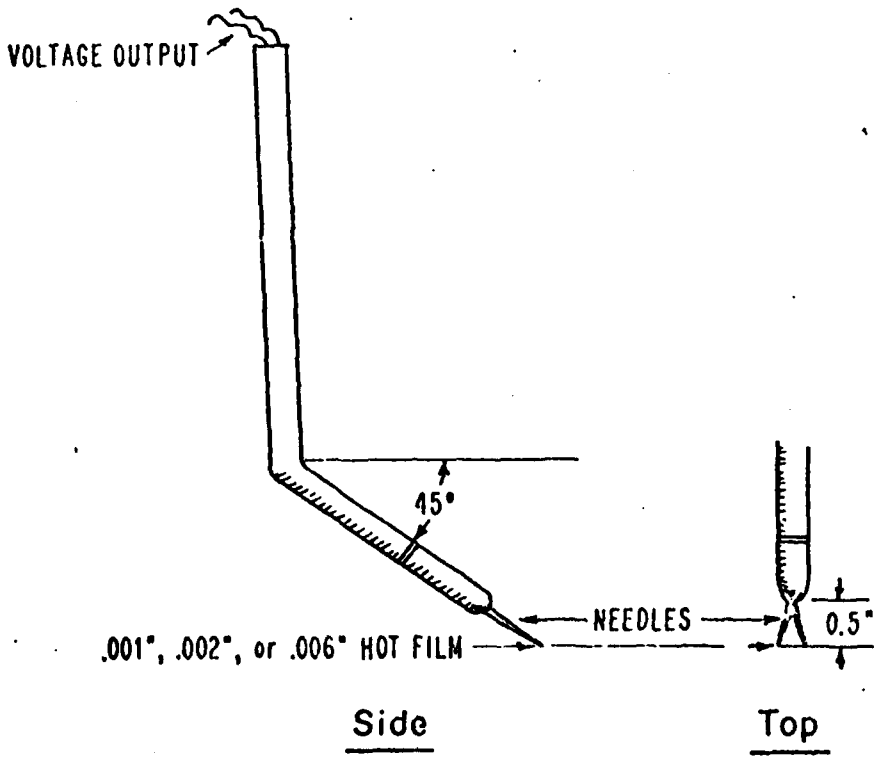

FIG. 5 THE HOT FILM PROBE

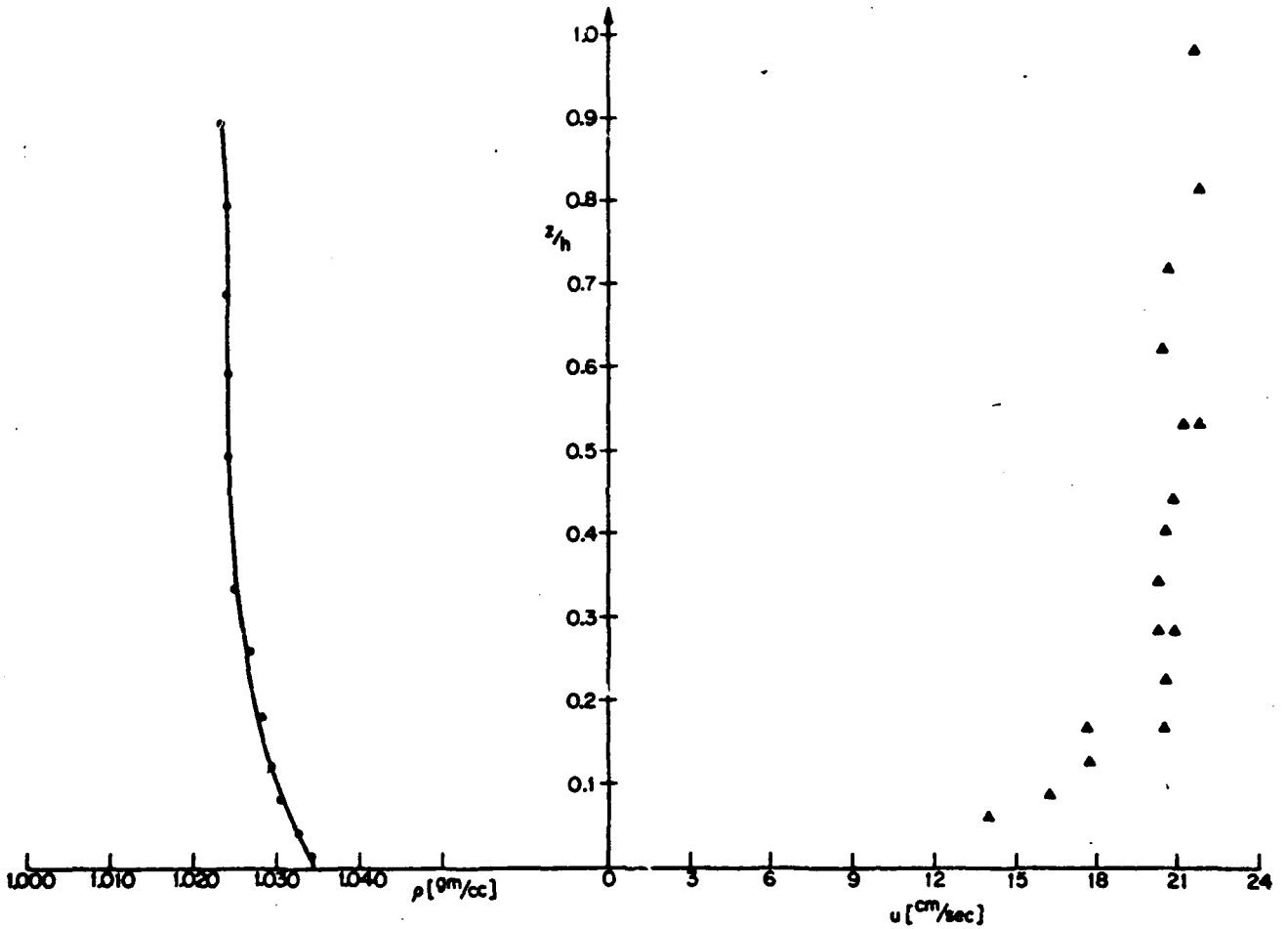

FIG. 6 PITOT TUBE VELOCITY PROFILES AND DENSITY PROFILES. Re. No. = 10,570 ; Ri. No. = .115

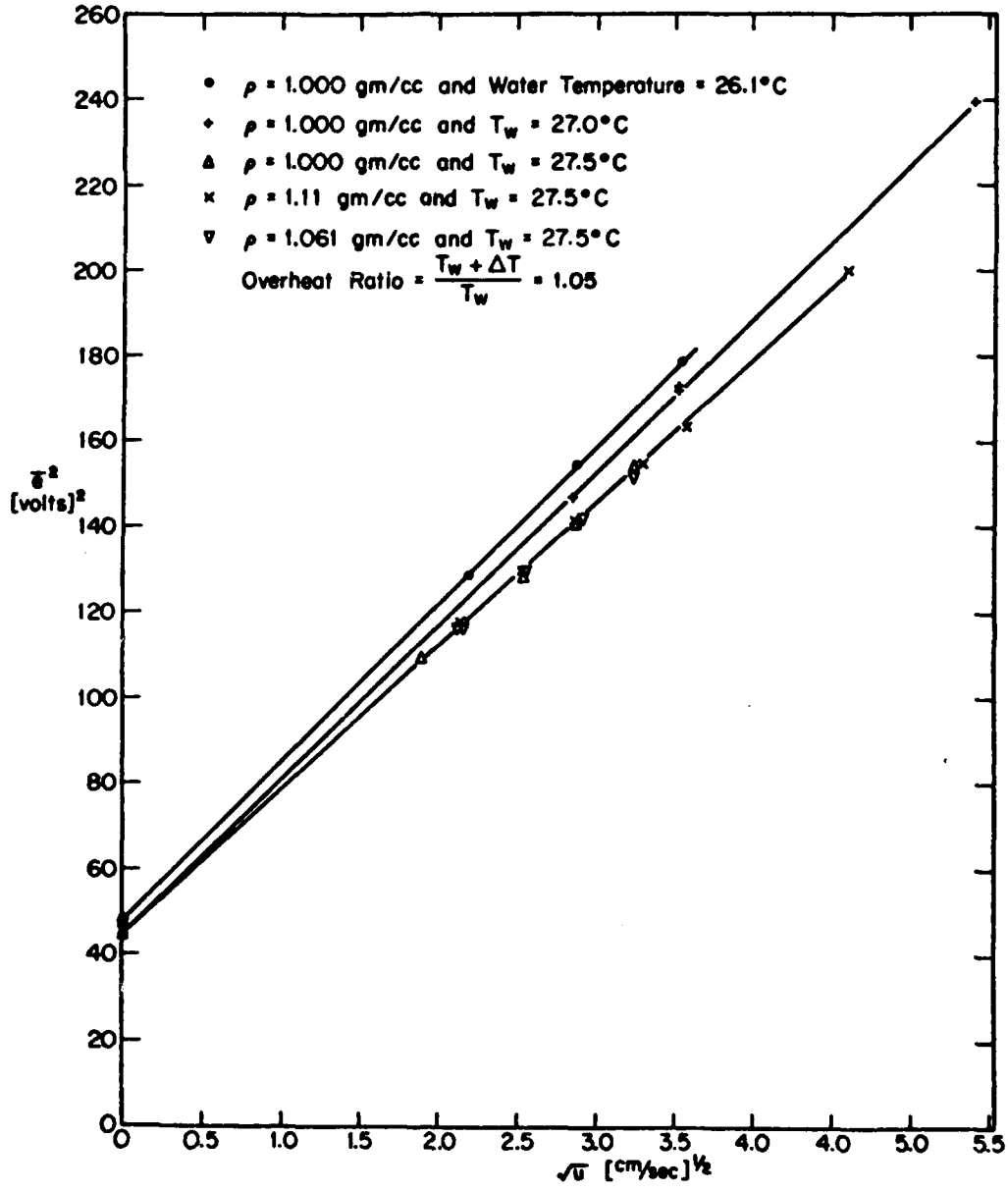

FIG. 7 HOT FILM CALIBRATION

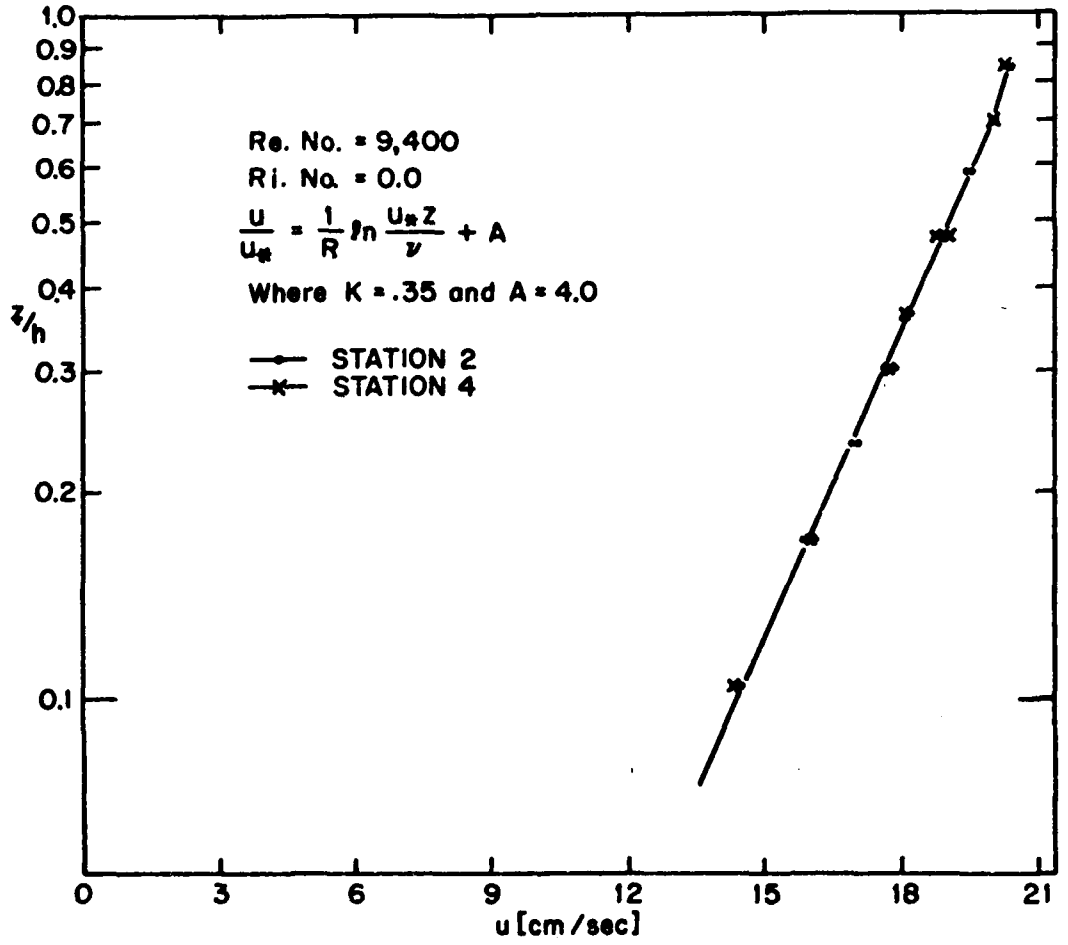

FIG. 8 MEAN VELOCITY vs. NORMALIZED DEPTH

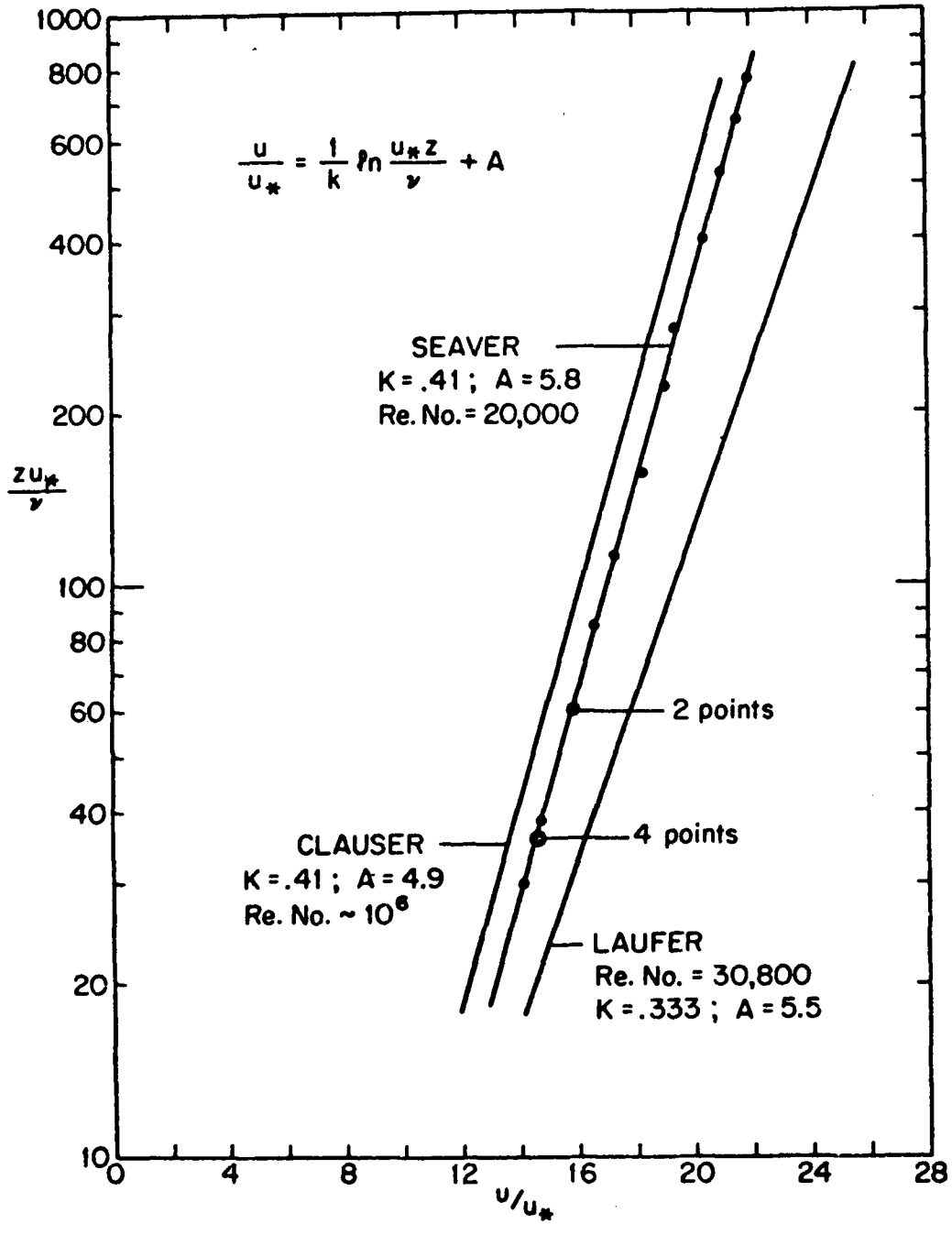

FIG. 9 TURBULENT LAW OF THE WALL FROM VARIOUS INVESTIGATORS

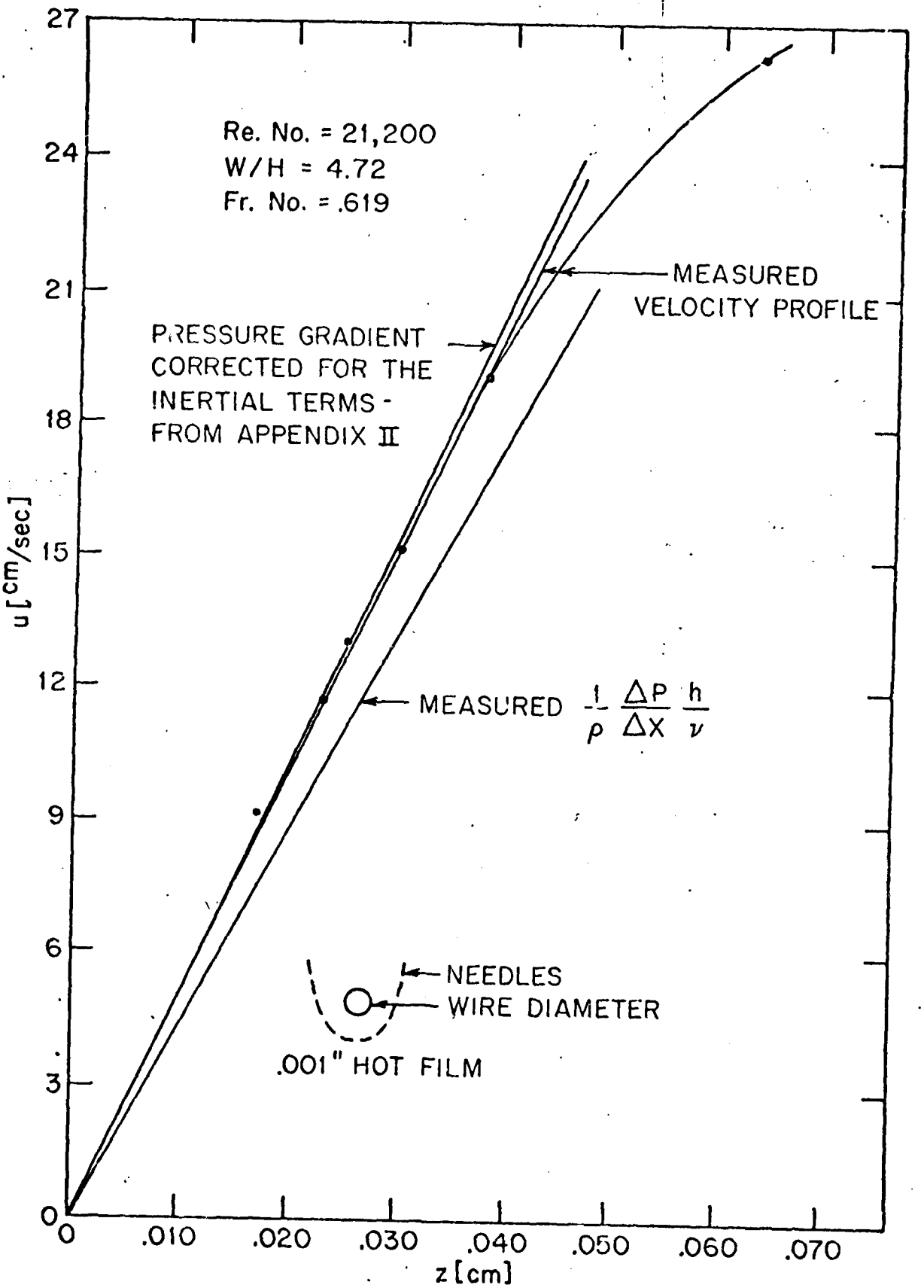

FIG. 10 SHEAR NEAR THE WALL

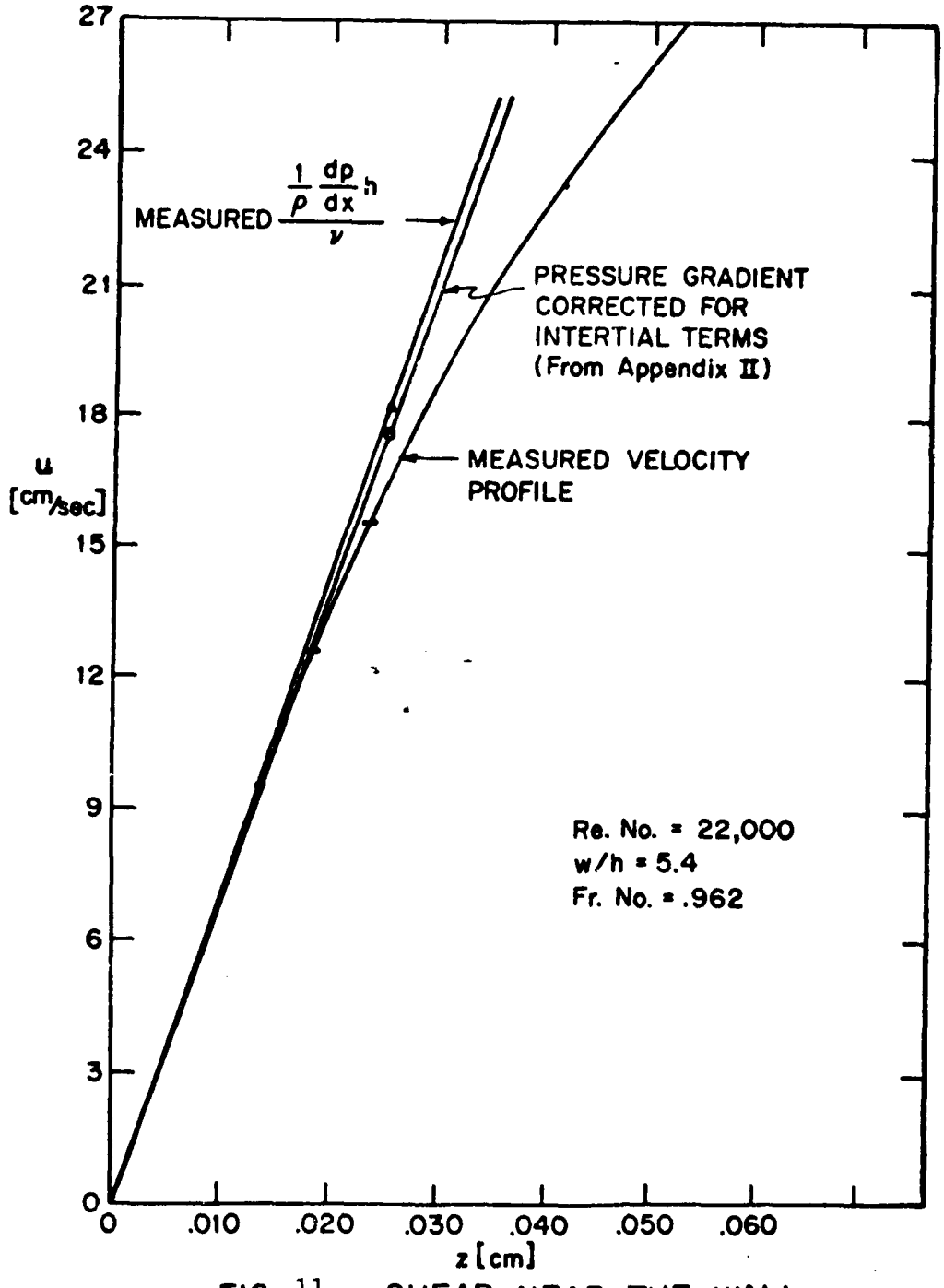

FIG. 11 SHEAR NEAR THE WALL

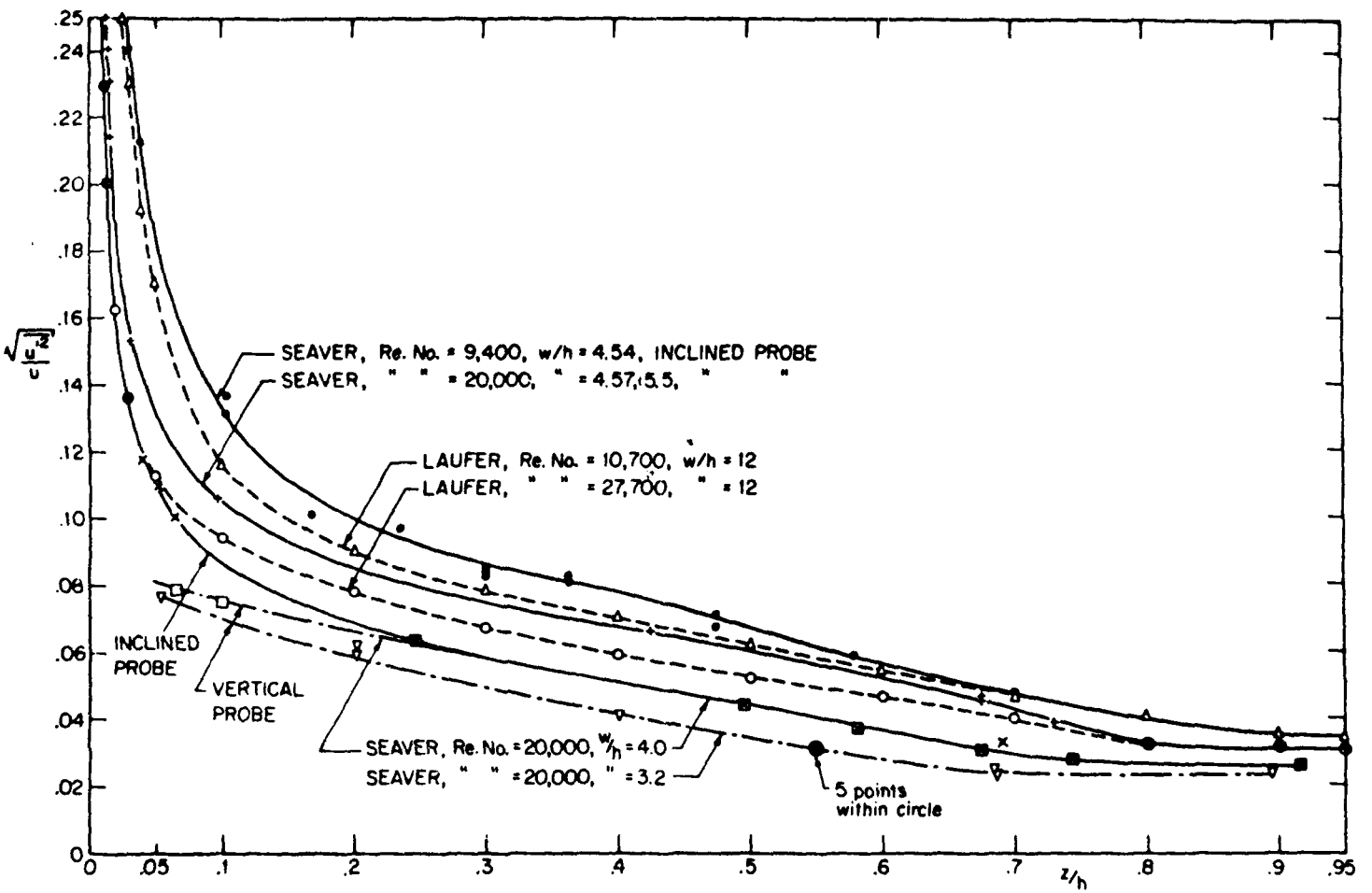

FIG. 12 R M S VELOCITY FLUCTUATION RELATIVE TO LOCAL MEAN VELOCITY FOR DIFFERENT ASPECT RATIOS AND Re. Nos.

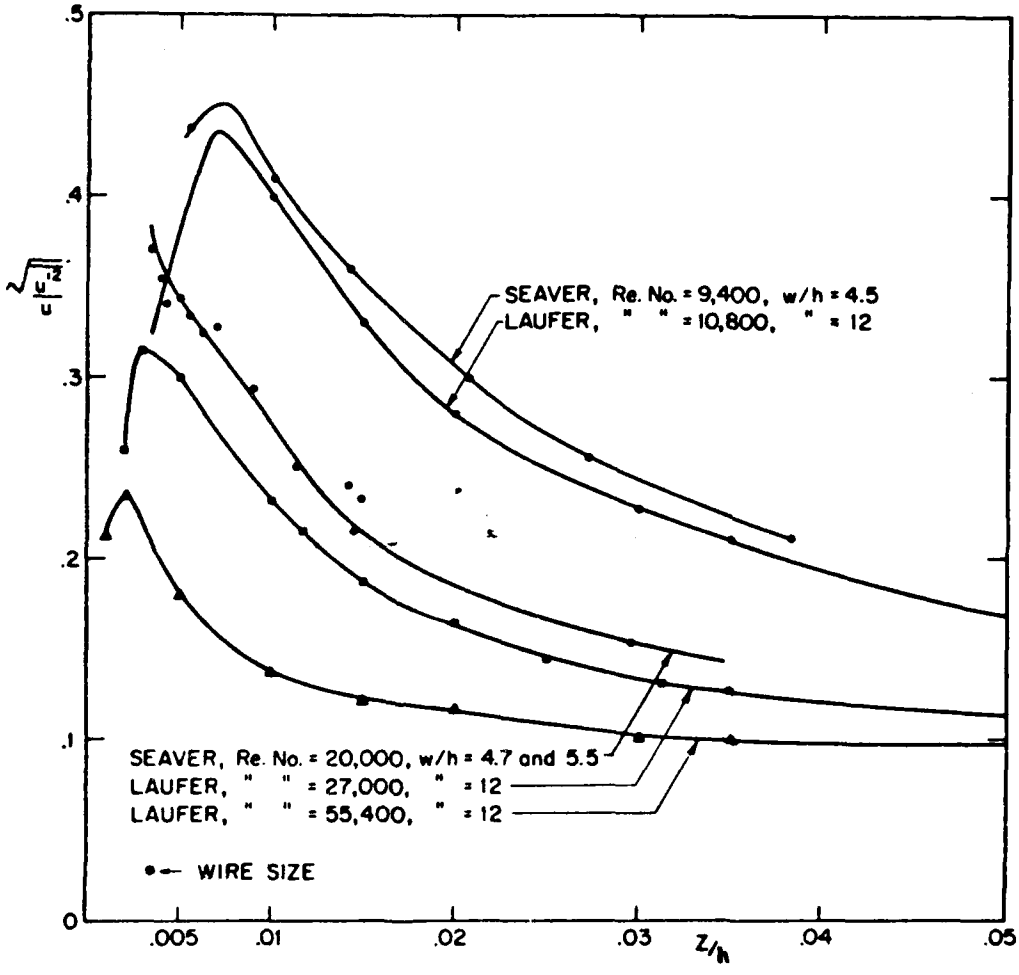

FIG. 3 NORMALIZED RMS FLUCTUATING VELOCITY vs. NORMALIZED DEPTH NEAR THE WALL FOR DIFFERENT ASPECT RATIOS AND Re. Nos.

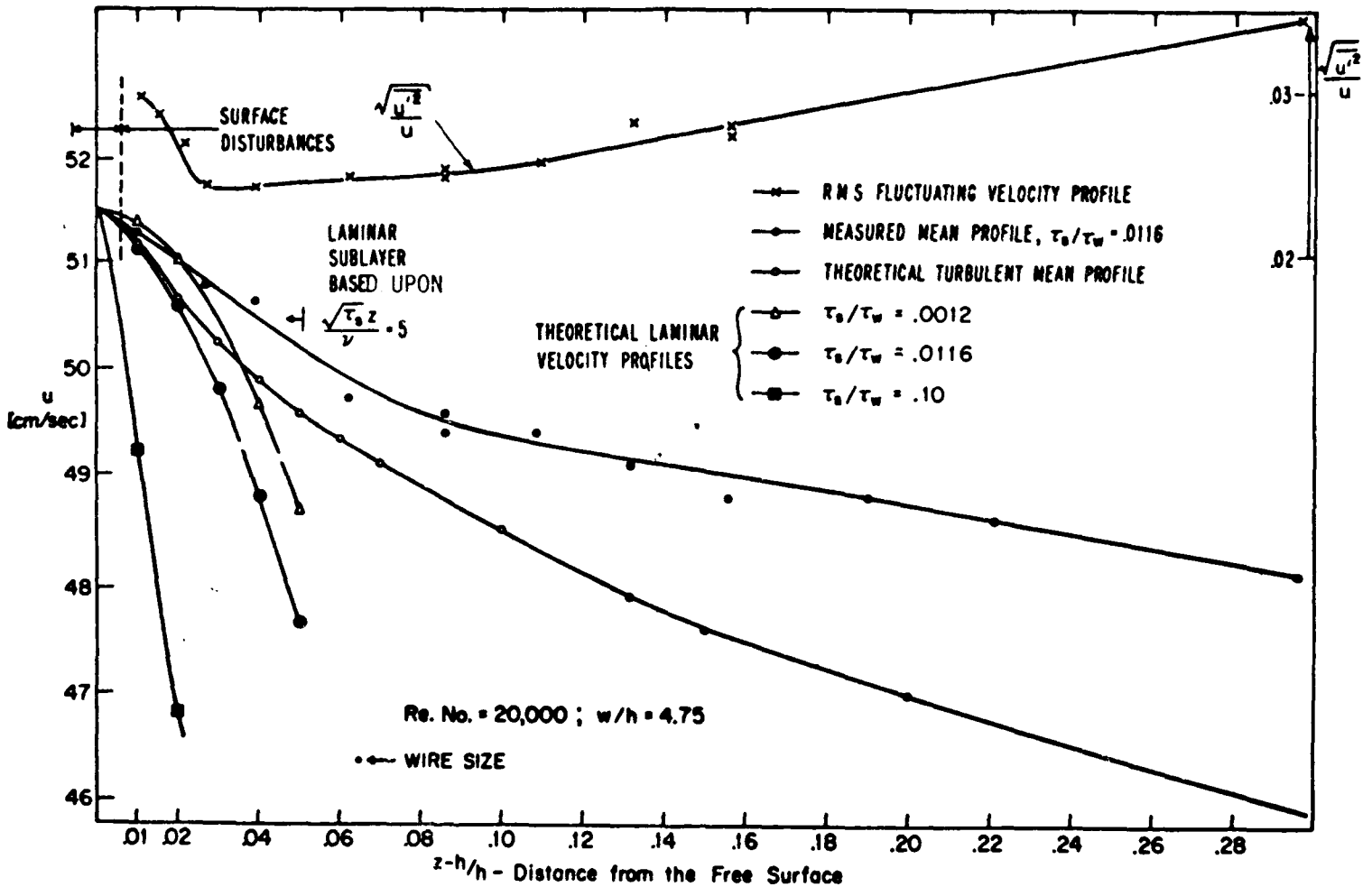

FIG. 14 VELOCITY NEAR THE FREE SURFACE

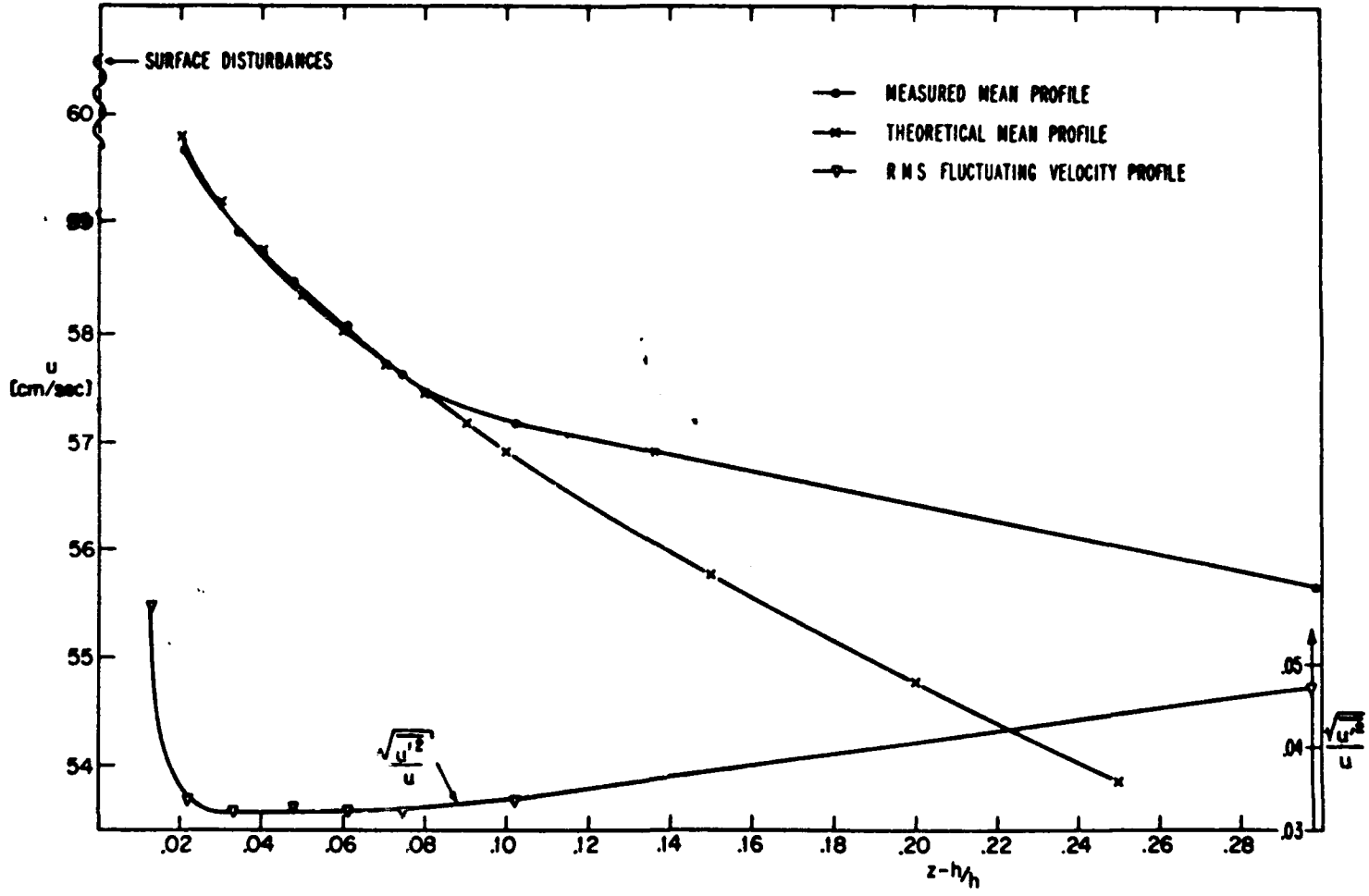

FIG. 15 VELOCITY NEAR THE FREE SURFACE $\tau_s/\tau_w = .022$; Re. No. = 20,000 ; w/h = 5.41

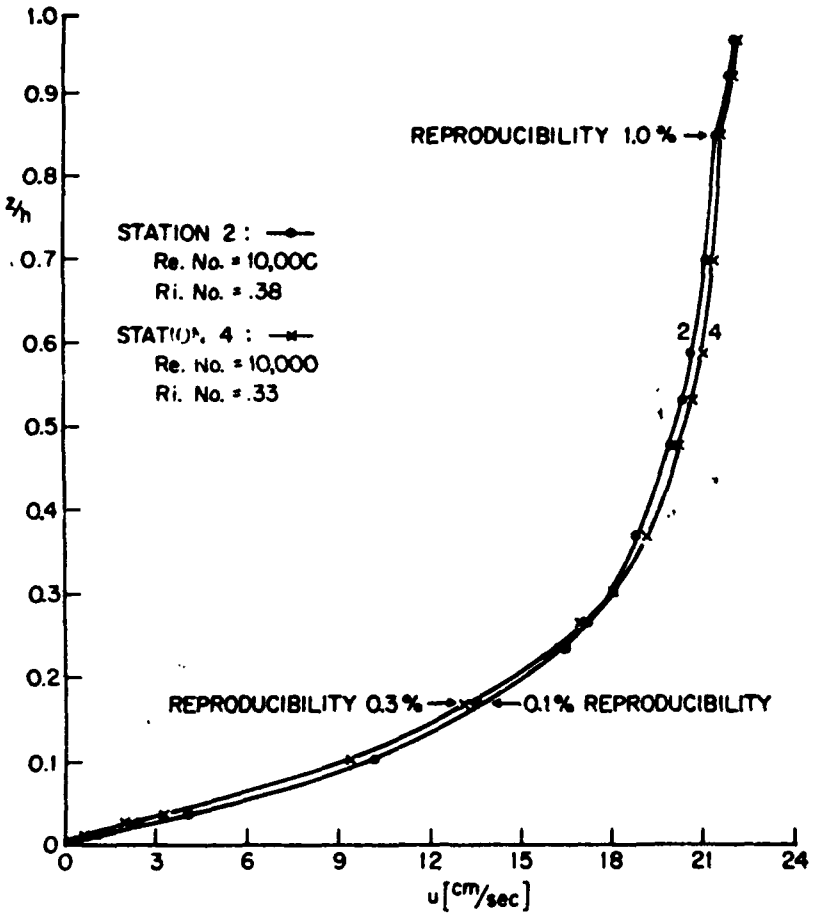

MEAN VELOCITY vs. NORMALIZED DEPTH

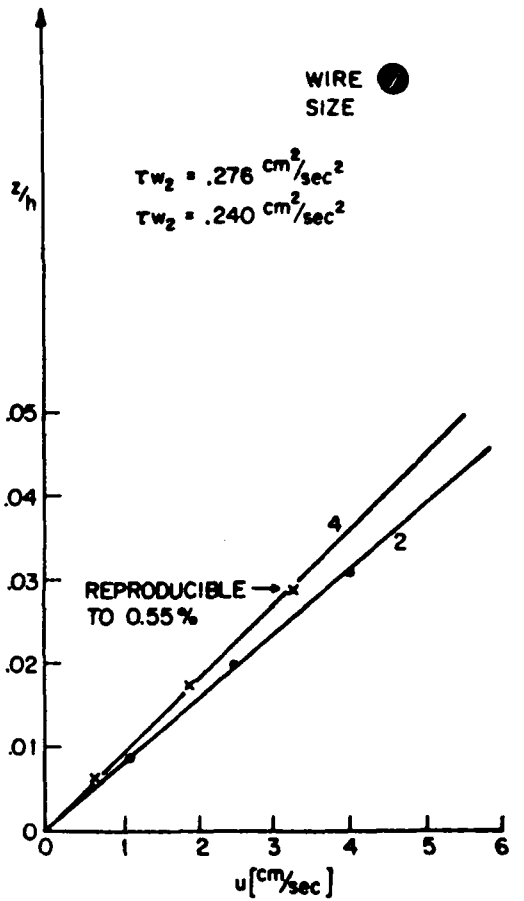

MEAN VELOCITY NEAR THE WALL vs. NORMALIZED DEPTH

FIGURE 16

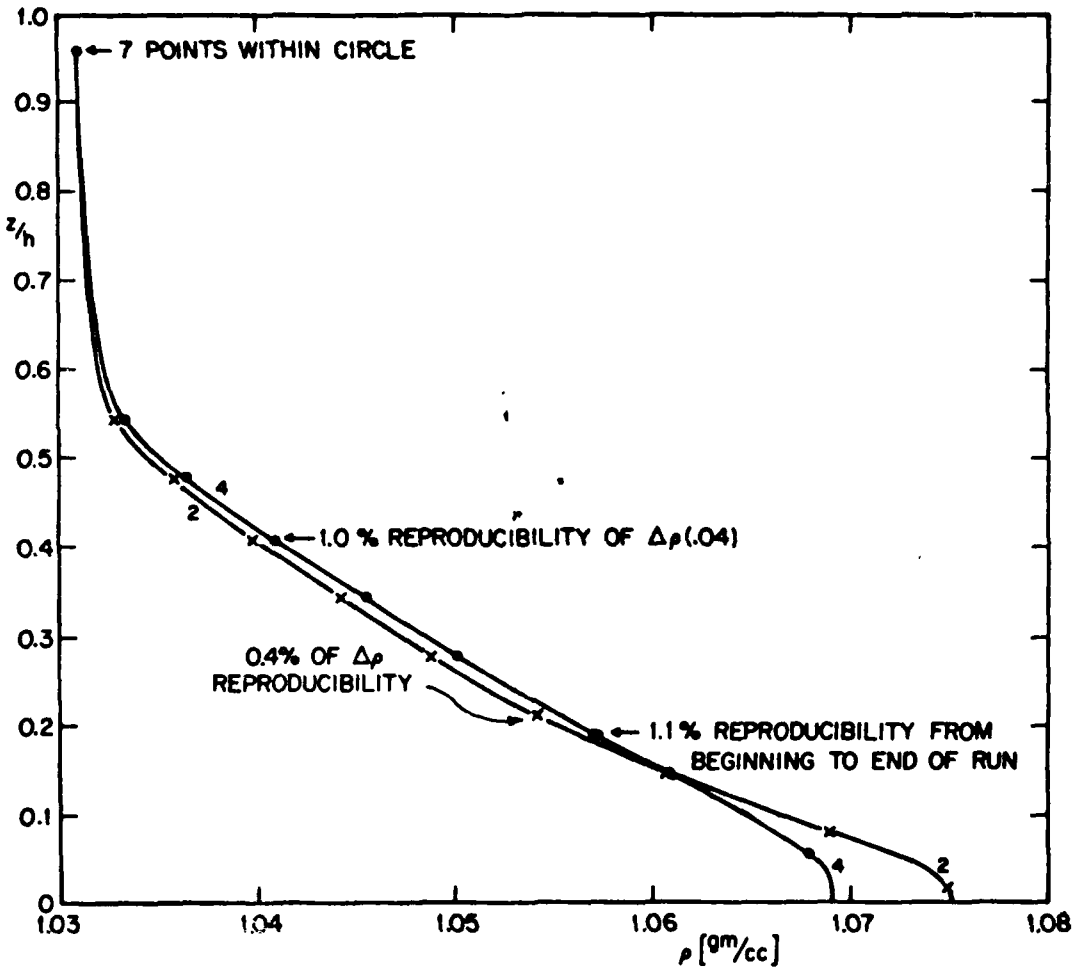

FIG. 17 MEAN DENSITY vs. NORMALIZED DEPTH

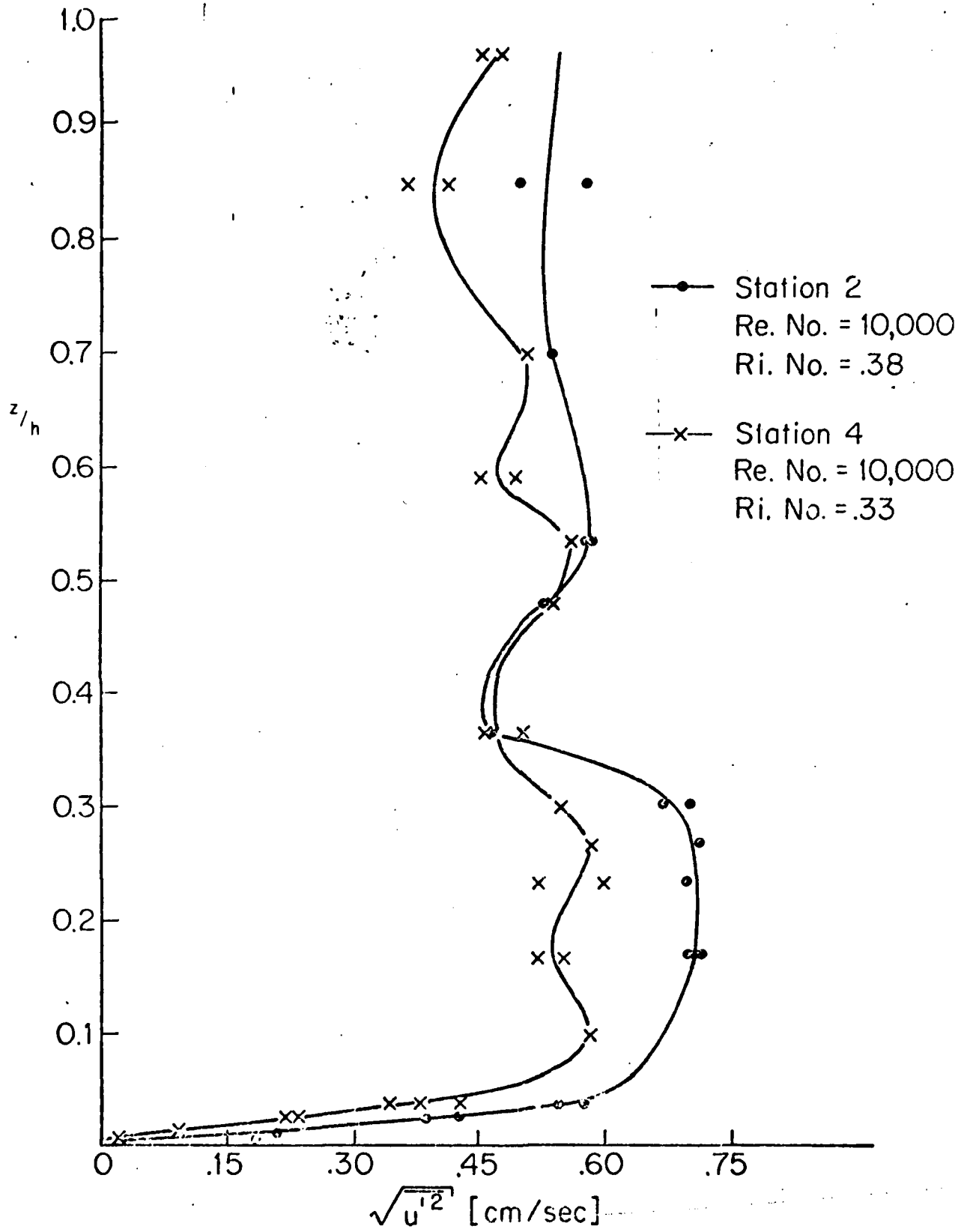

FIG. 18 RMS FLUCTUATING VELOCITY vs. NORMALIZED DEPTH

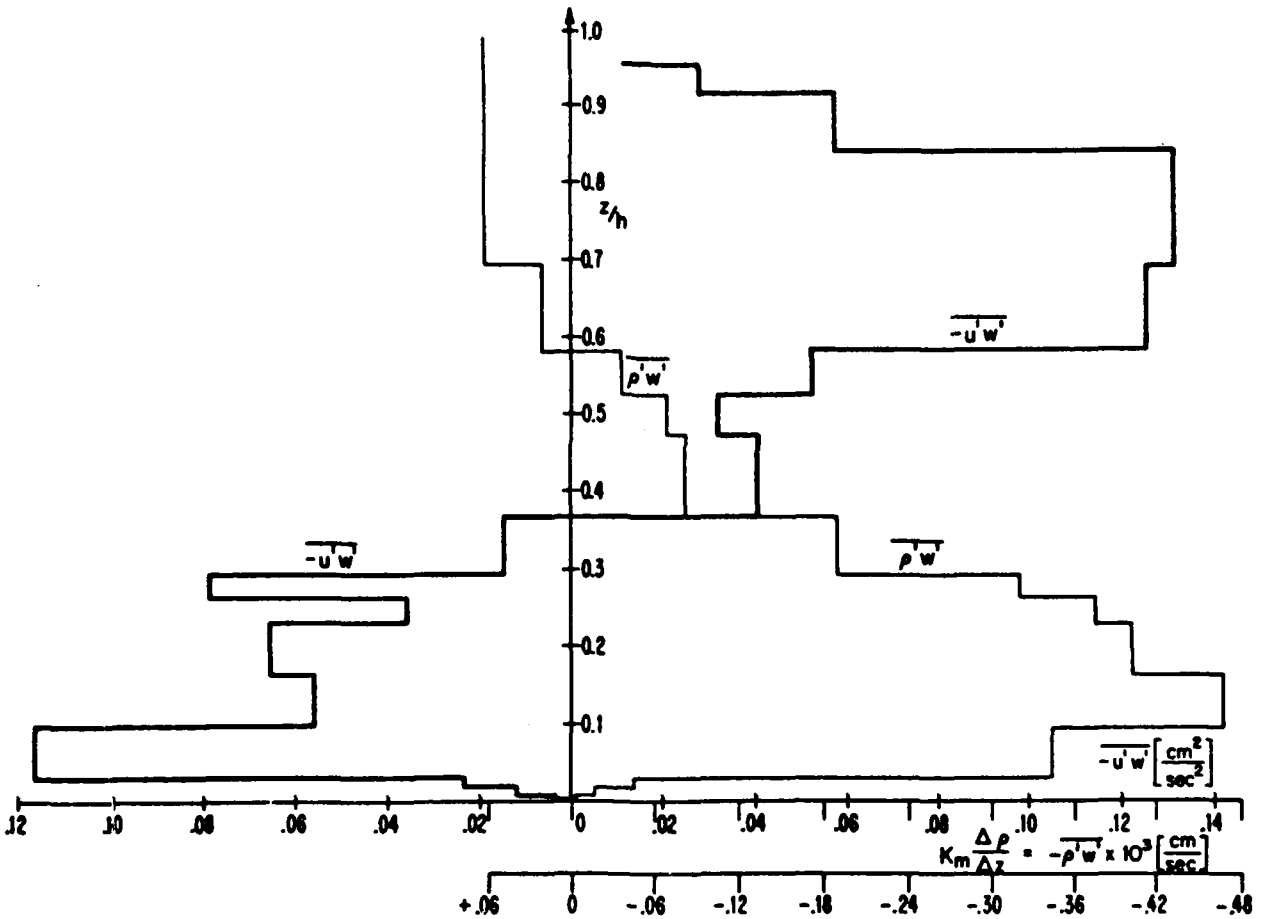

FIG. 19 SALT FLUX AND REYNOLDS STRESS vs. NORMALIZED DEPTH. Re. No. = 10,100 ; Ri. No. = .33
DOWNSTREAM STATION 4

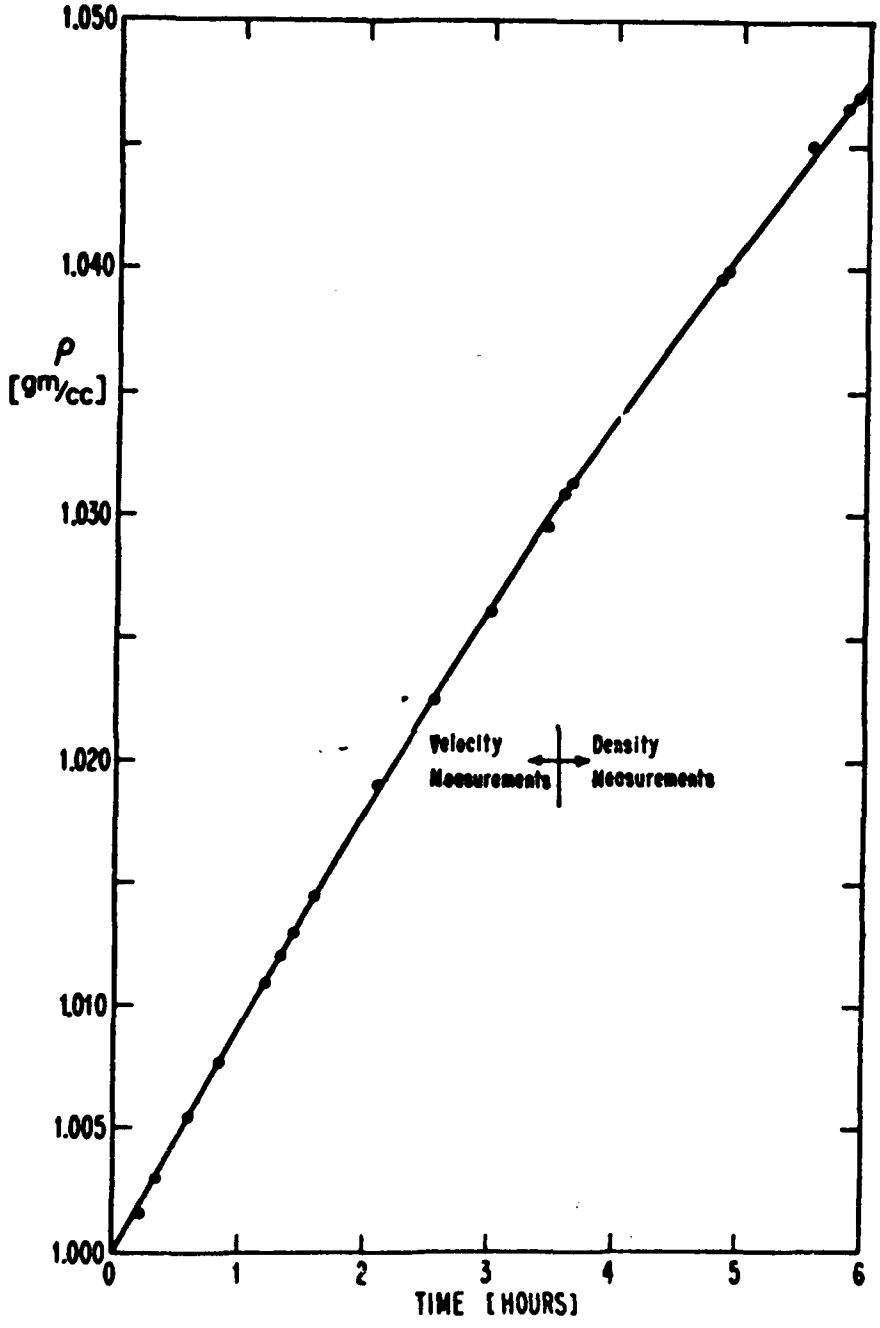

FIG. 20 THE RATE OF INCREASE OF THE AMBIENT DENSITY. $\Delta\rho/\Delta t = 1.149 \times 10^{-4}$ gm/cc min.

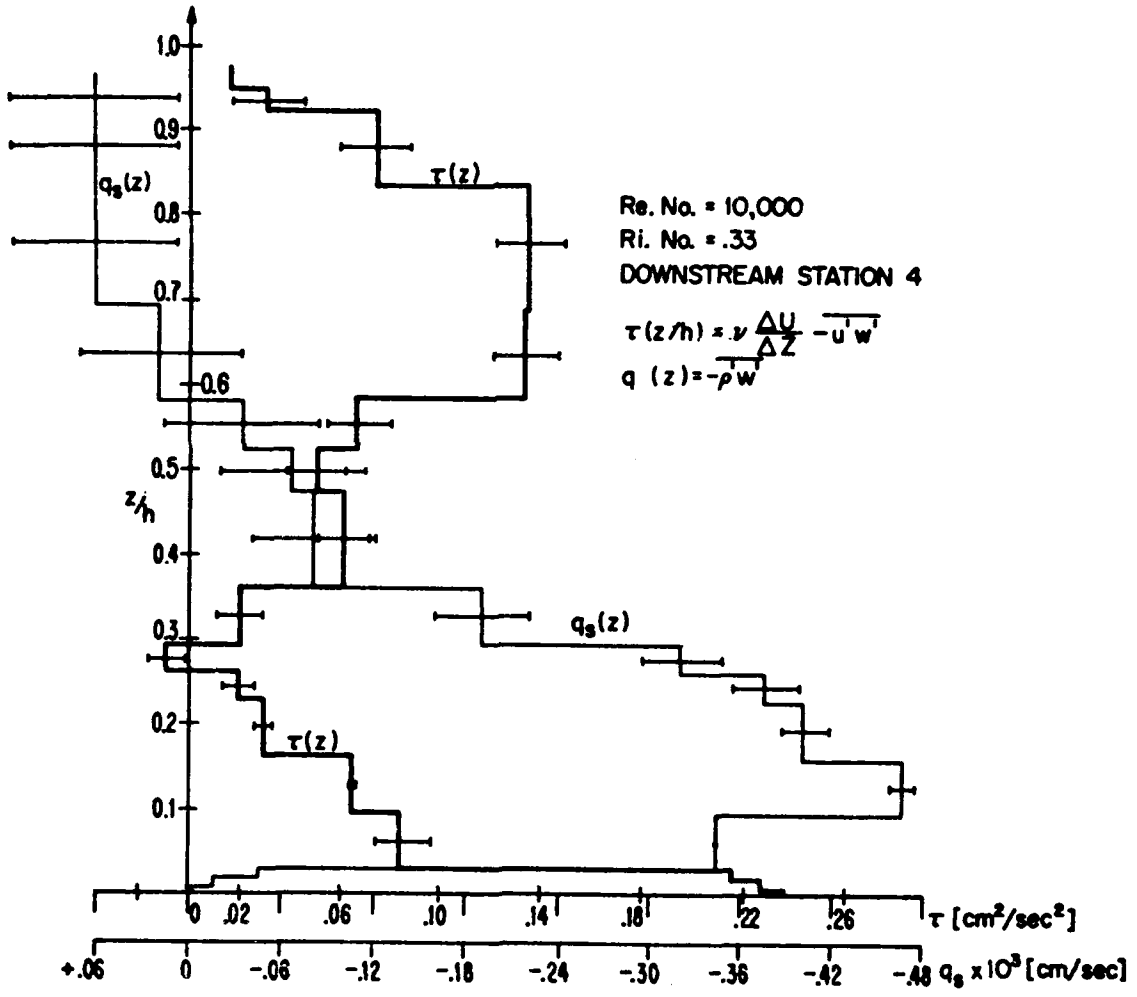

FIG. 21 MOMENTUM AND SALINITY FLUXES vs. NORMALIZED DEPTH

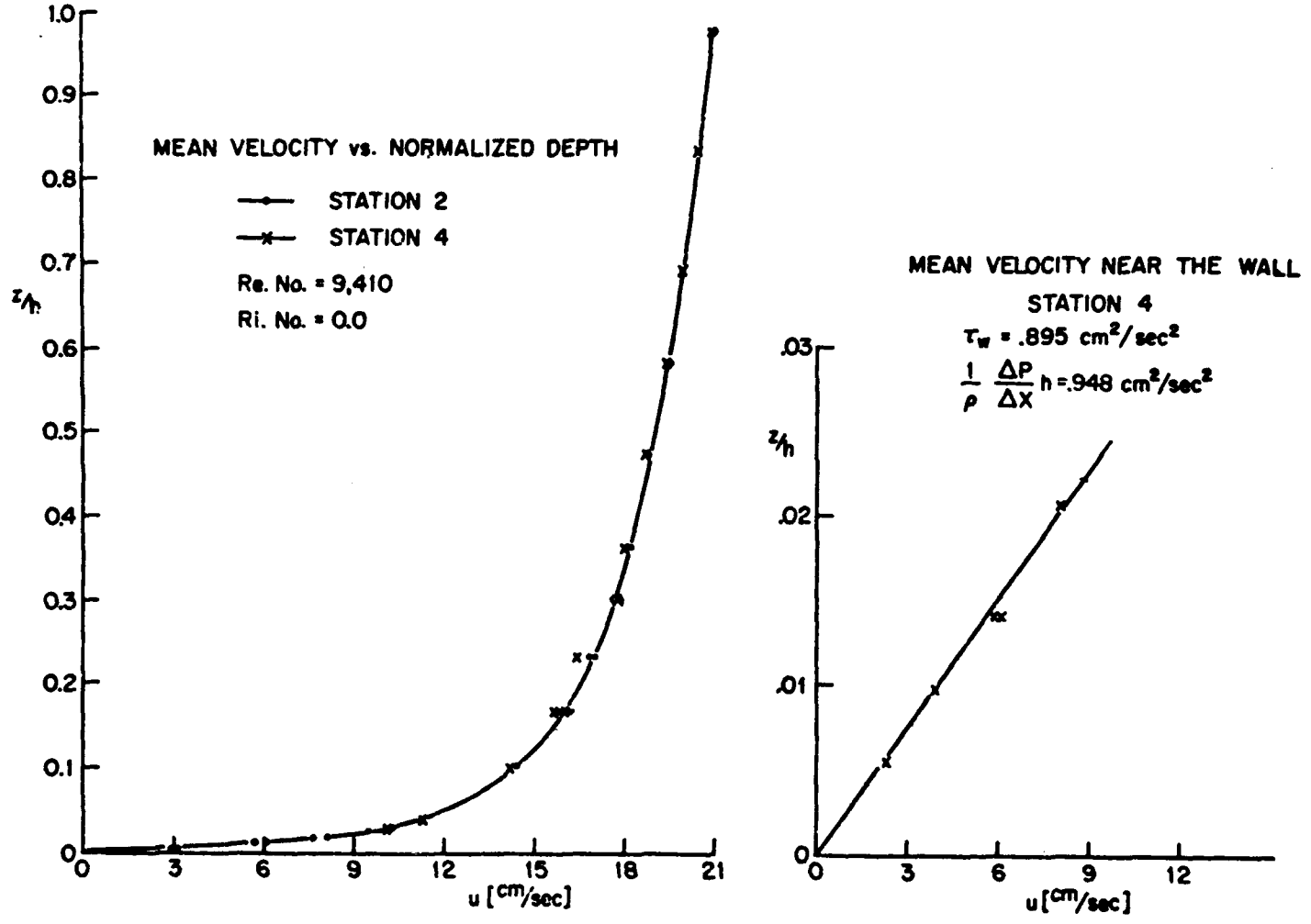
MEAN VELOCITY vs. NORMALIZED DEPTH
STATION 2
STATION 4
Re. No. = 9,410
Ri. No. = 0.0
z/h
u [cm/sec]
MEAN VELOCITY NEAR THE WALL
STATION 4
τ_w = .895 cm²/sec²
$\frac{1}{\rho}\frac{\Delta P}{\Delta X}$ h = .948 cm²/sec²
z/h
u [cm/sec]

FIGURE 22

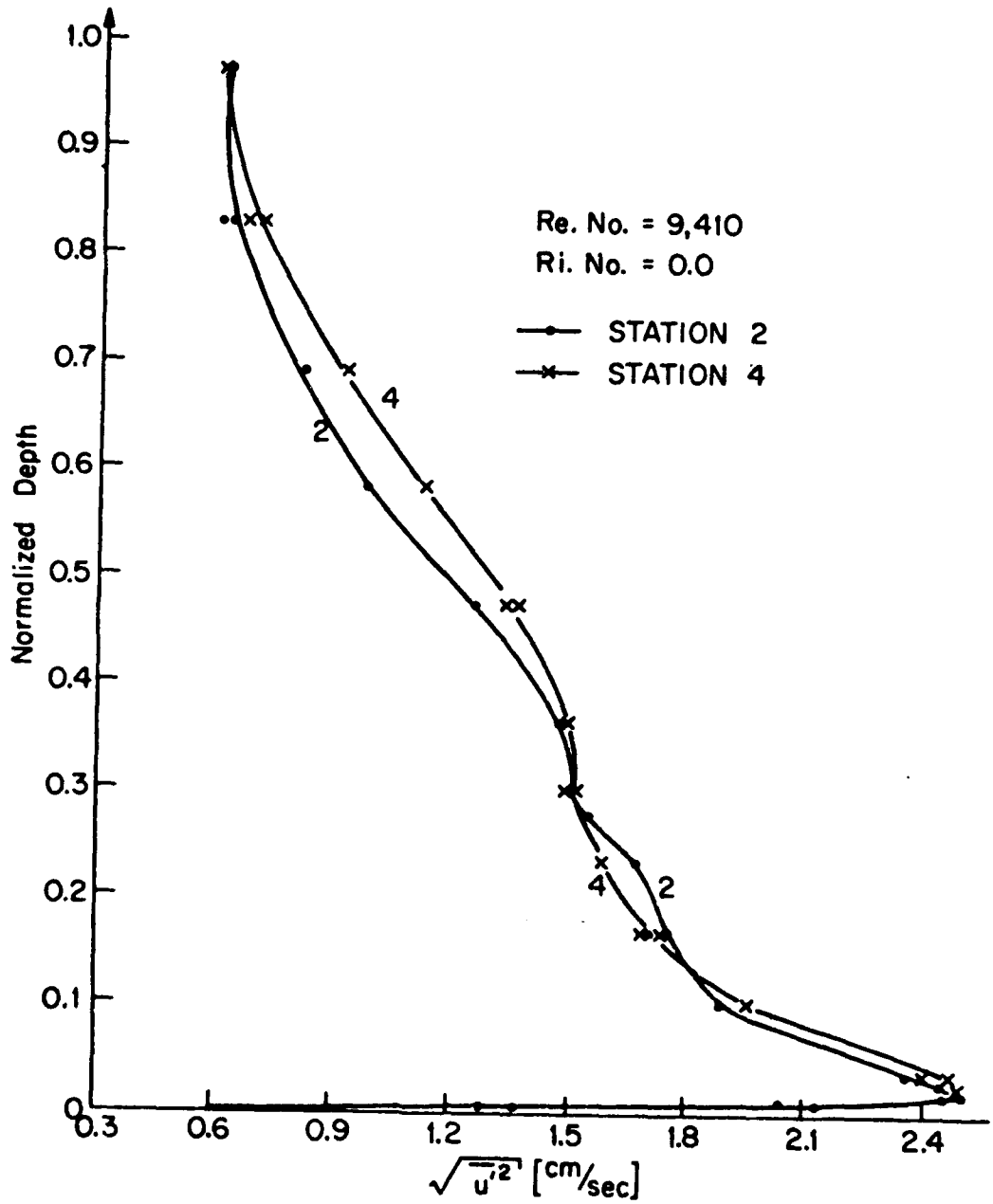

FIG. 23 FLUCTUATING VELOCITY PROFILE vs. DEPTH

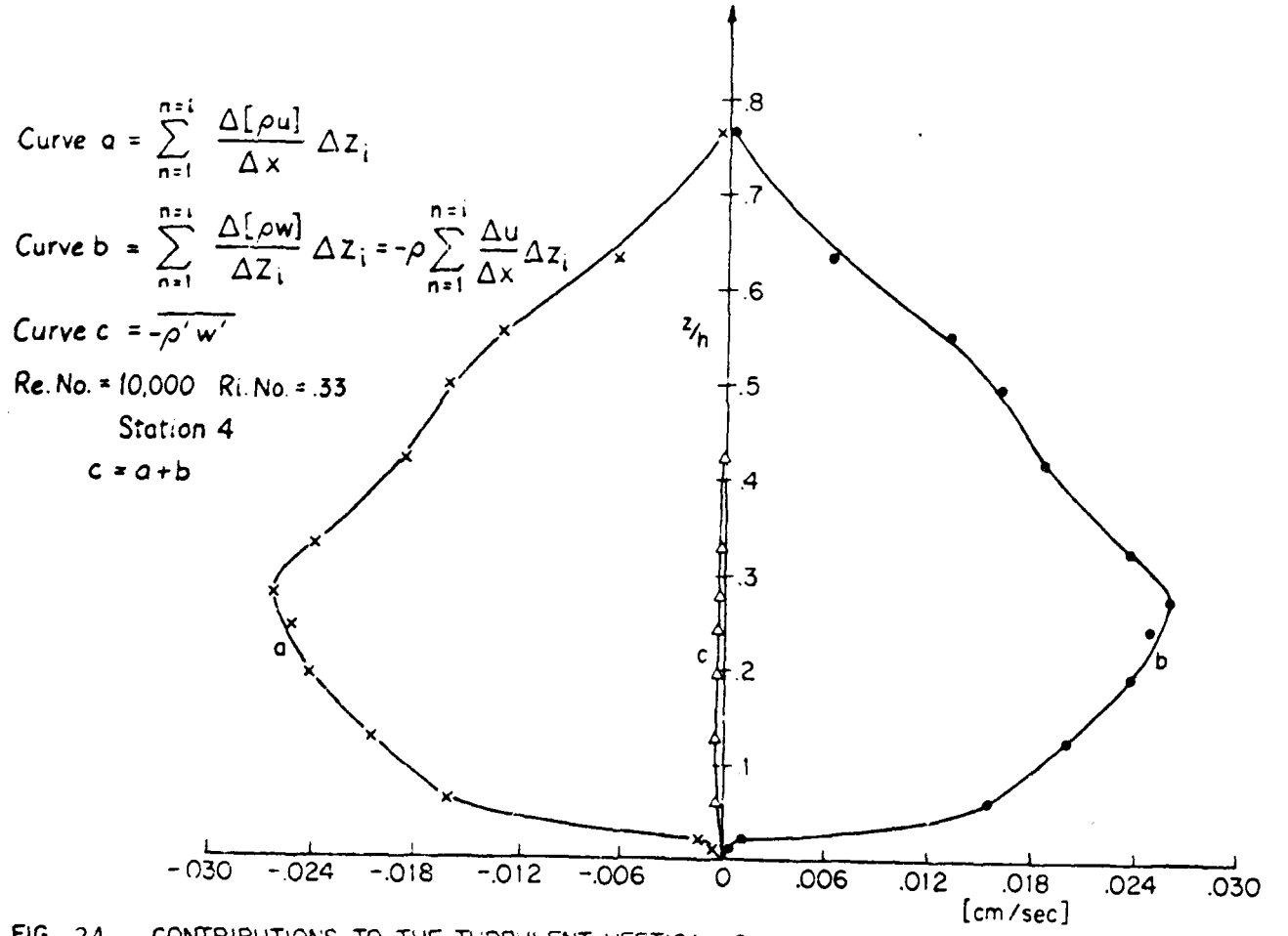

FIG. 24 CONTRIBUTIONS TO THE TURBULENT VERTICAL SALT FLUX FROM THE MEAN VERTICAL FLUX AND THE INTEGRATED HORIZONTAL FLUX DIVERGENGE

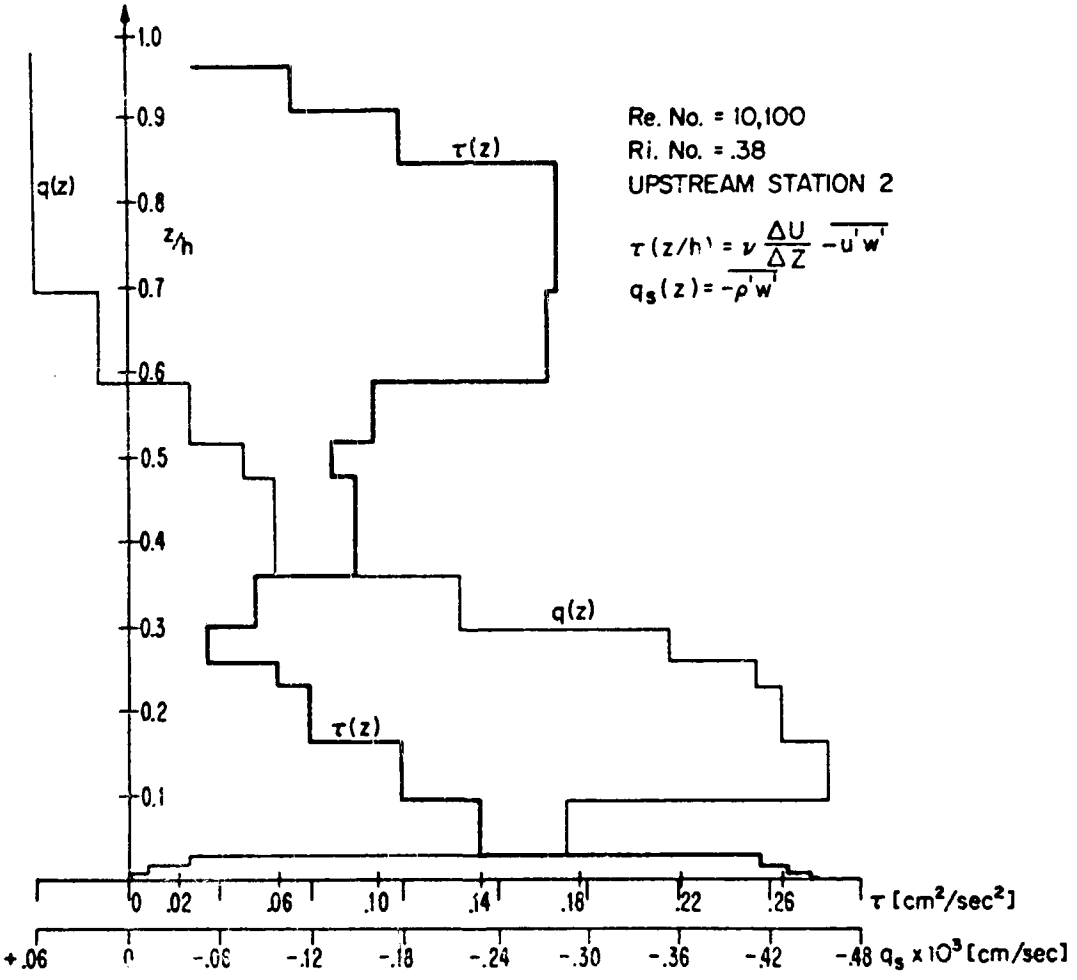

FIG. 25 MOMENTUM AND SALINITY FLUXES vs. NORMALIZED DEPTH

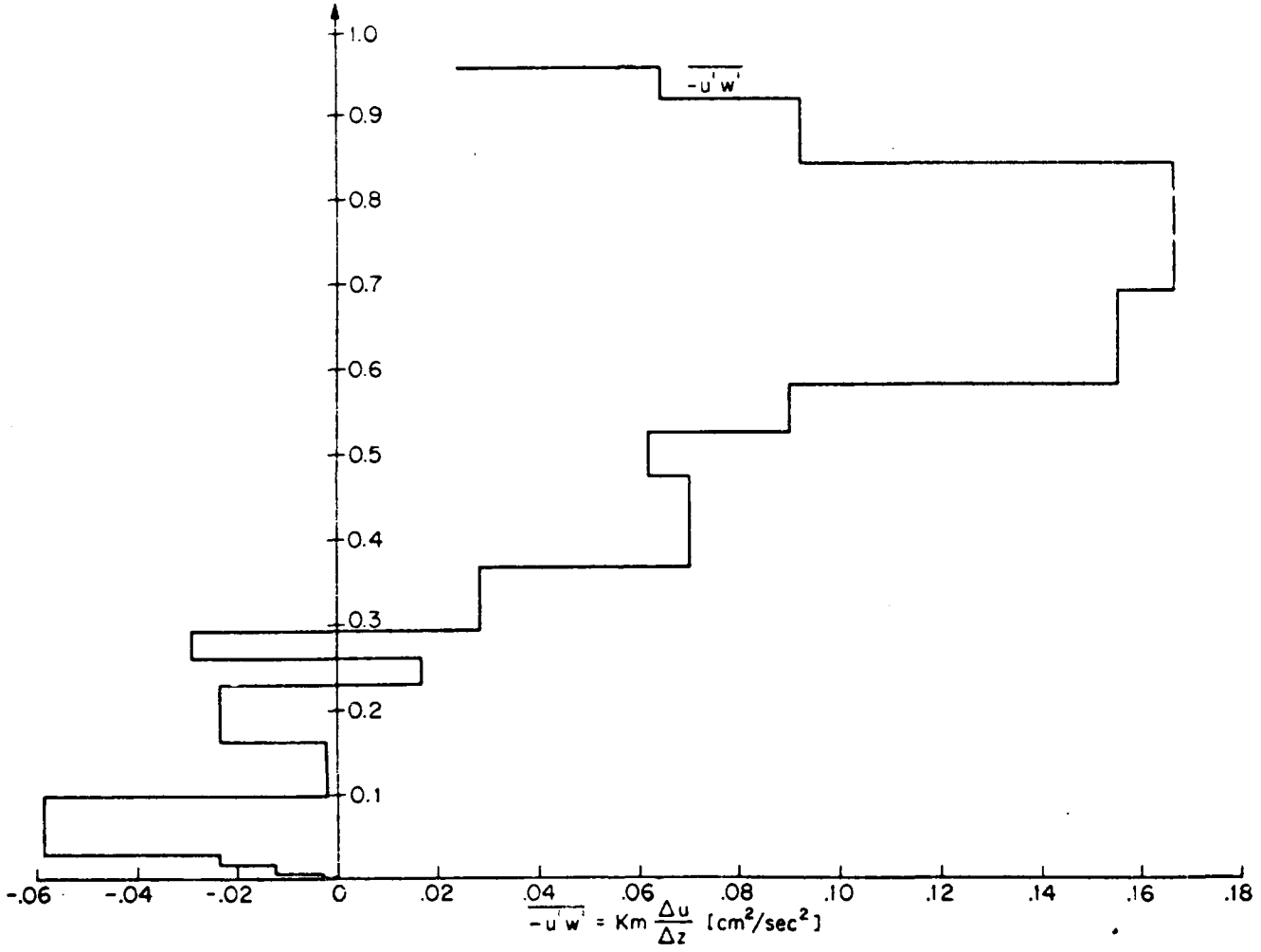

FIG. 26 REYNOLDS STRESS vs. DEPTH UPSTREAM STATION 2 . Re. No. = 10,000 ; Ri. No. = .38

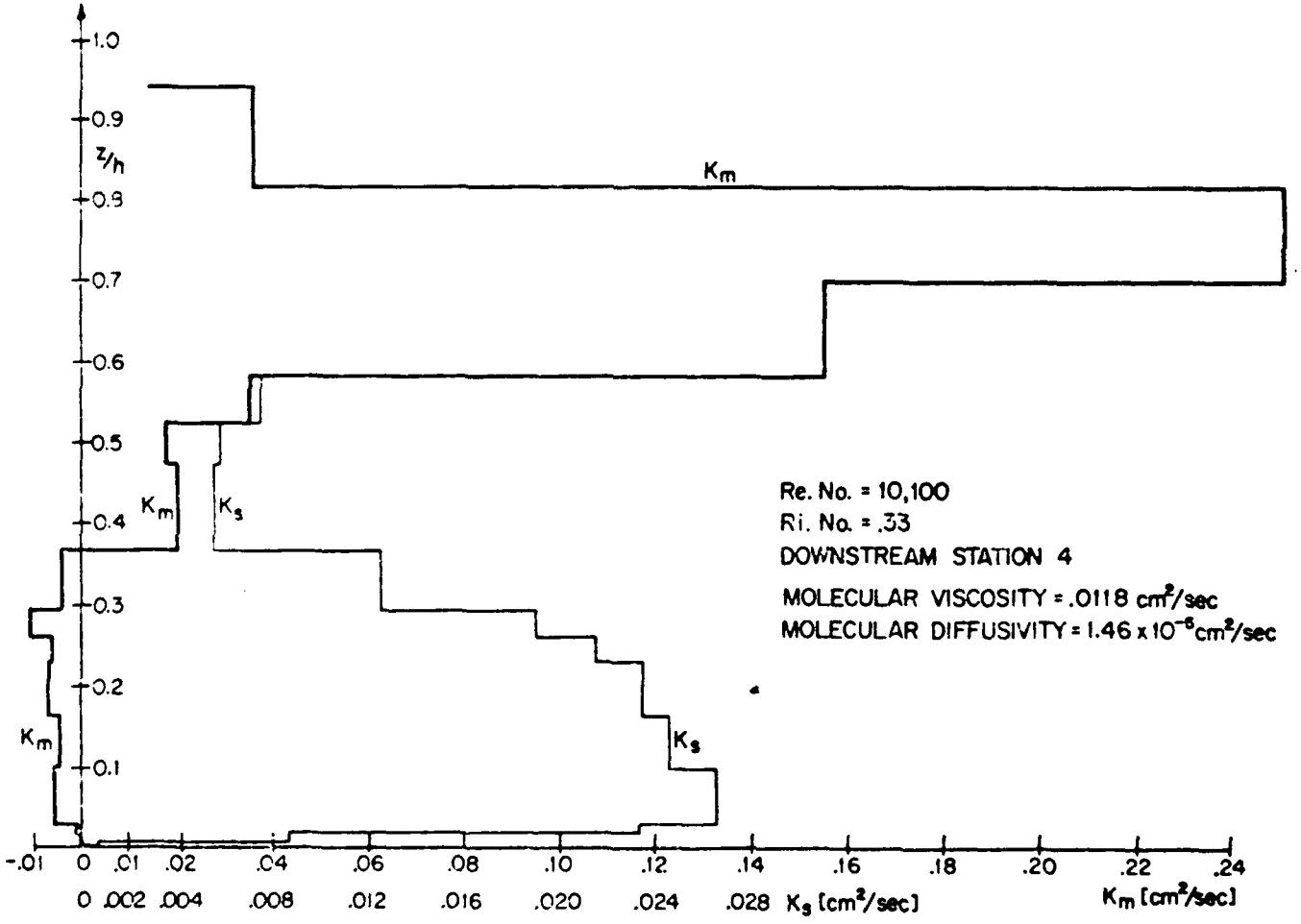

FIG. 27 MOMENTUM AND SALINITY AUSTAUSCH COEFFICIENTS vs. DEPTH

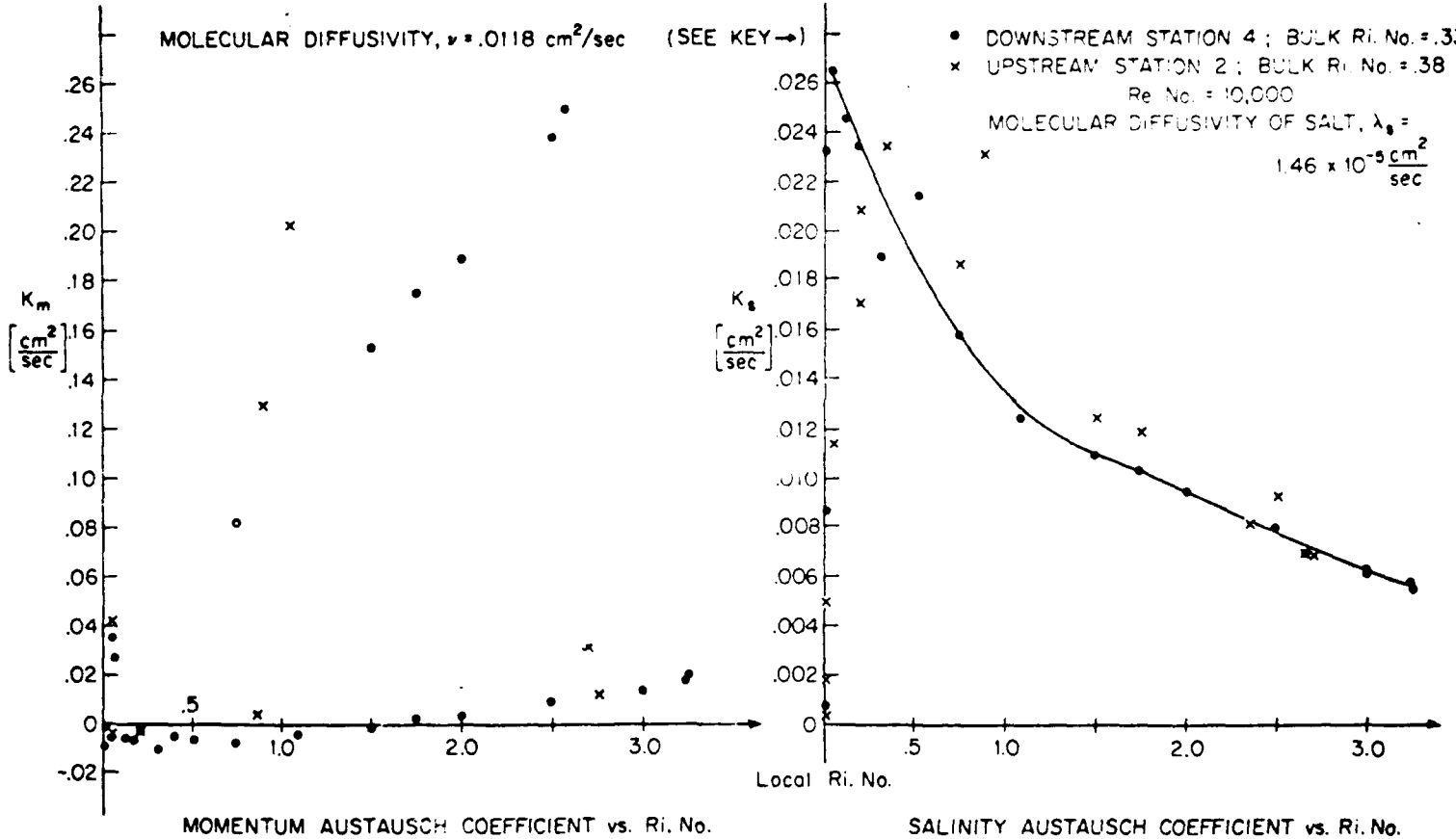

MOMENTUM AUSTAUSCH COEFFICIENT vs. Ri. No.

SALINITY AUSTAUSCH COEFFICIENT vs. Ri. No.

FIGURE 28

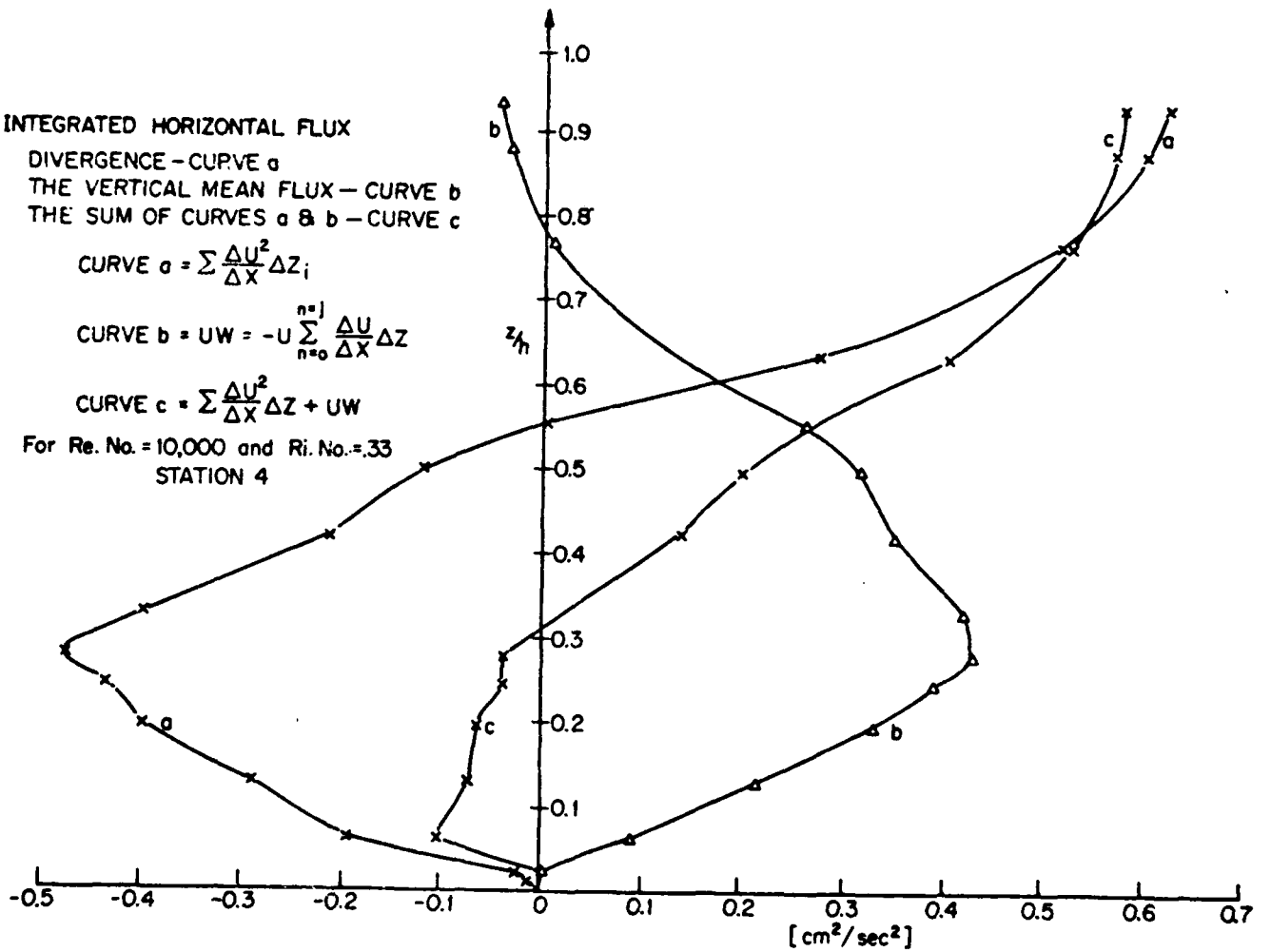

FIG. 29 THE DEPENDENCE ON THE NORMALIZED DEPTH OF THE ADVECTIVE FLUXES

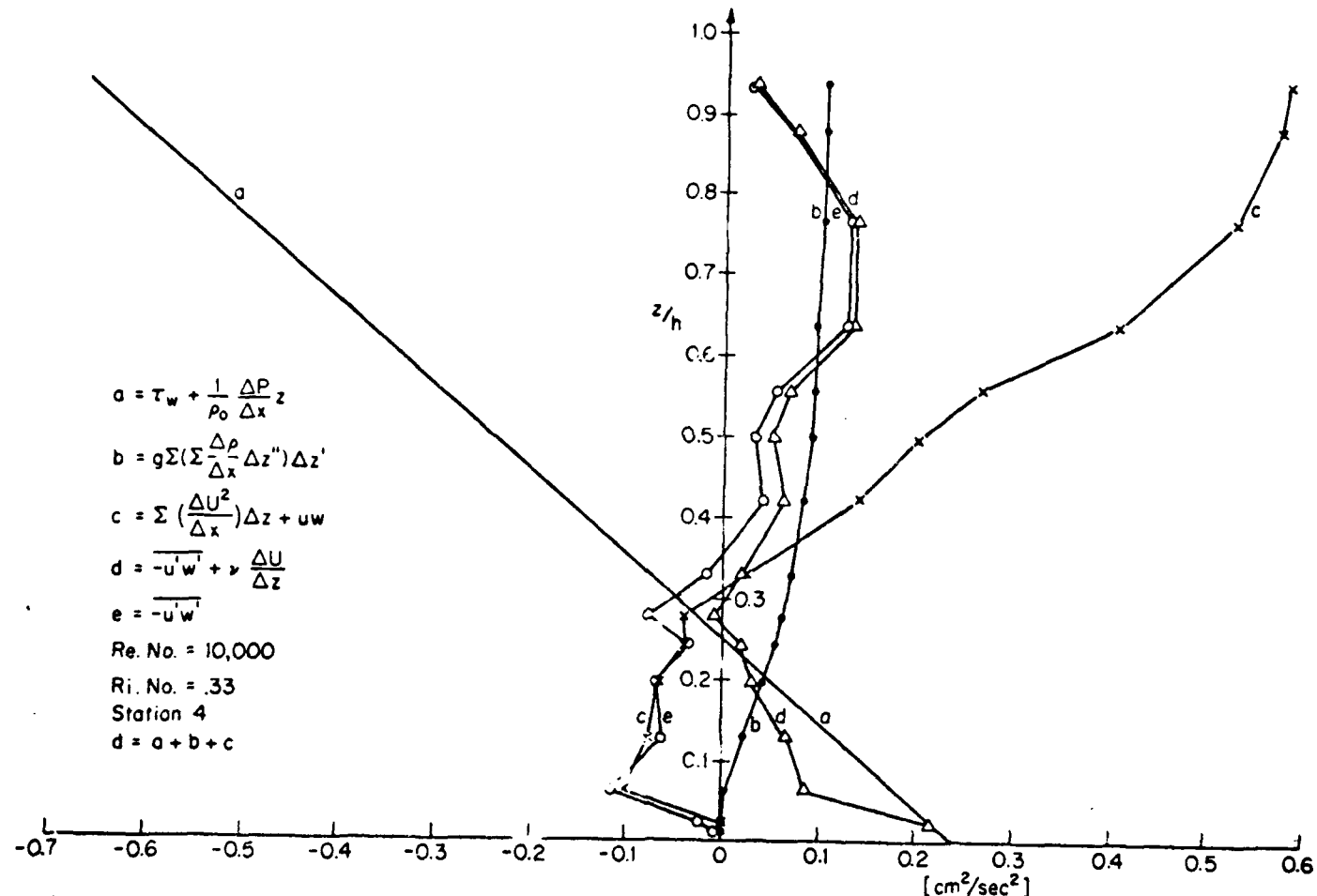

FIG. 30 CONTRIBUTIONS TO THE TOTAL SHEAR (CURVE d) FROM THE WALL SHEAR AND PRESSURE GRADIENT (CURVE a), BAROCLINIC PRESSURE GRADIENT (CURVE b), MEAN ADVECTIVE FLUXES (CURVE c), AND TURBULENT VERTICAL MOMENTUM FLUX (CURVE e).

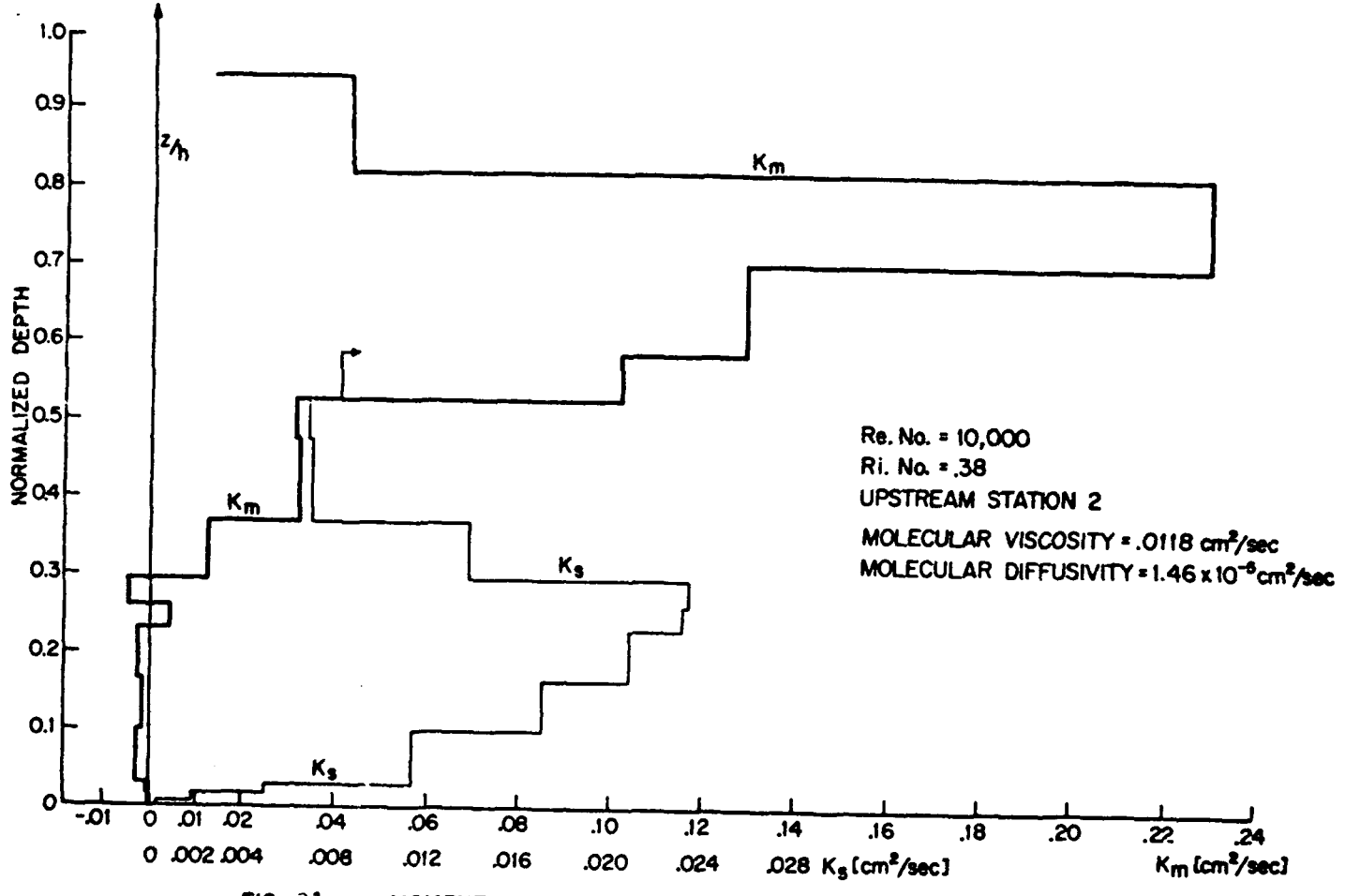

FIG. 31 MOMENTUM AND SALINITY AUSTAUSCH COEFFICIENTS vs. DEPTH

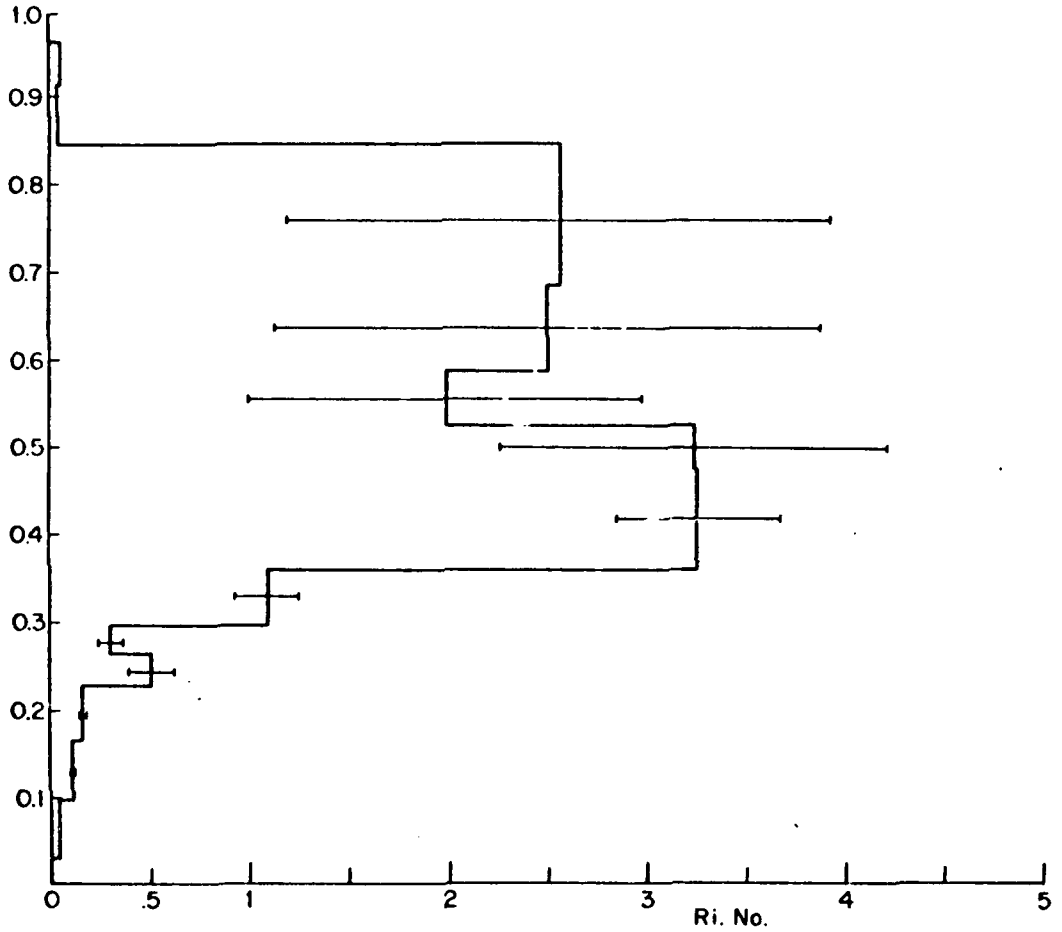

FIG. 32 LOCAL Ri. No. vs. NORMALIZED DEPTH DOWNSTREAM STATION 4
Re. No. = 10,000 ; Ri. No. = .33

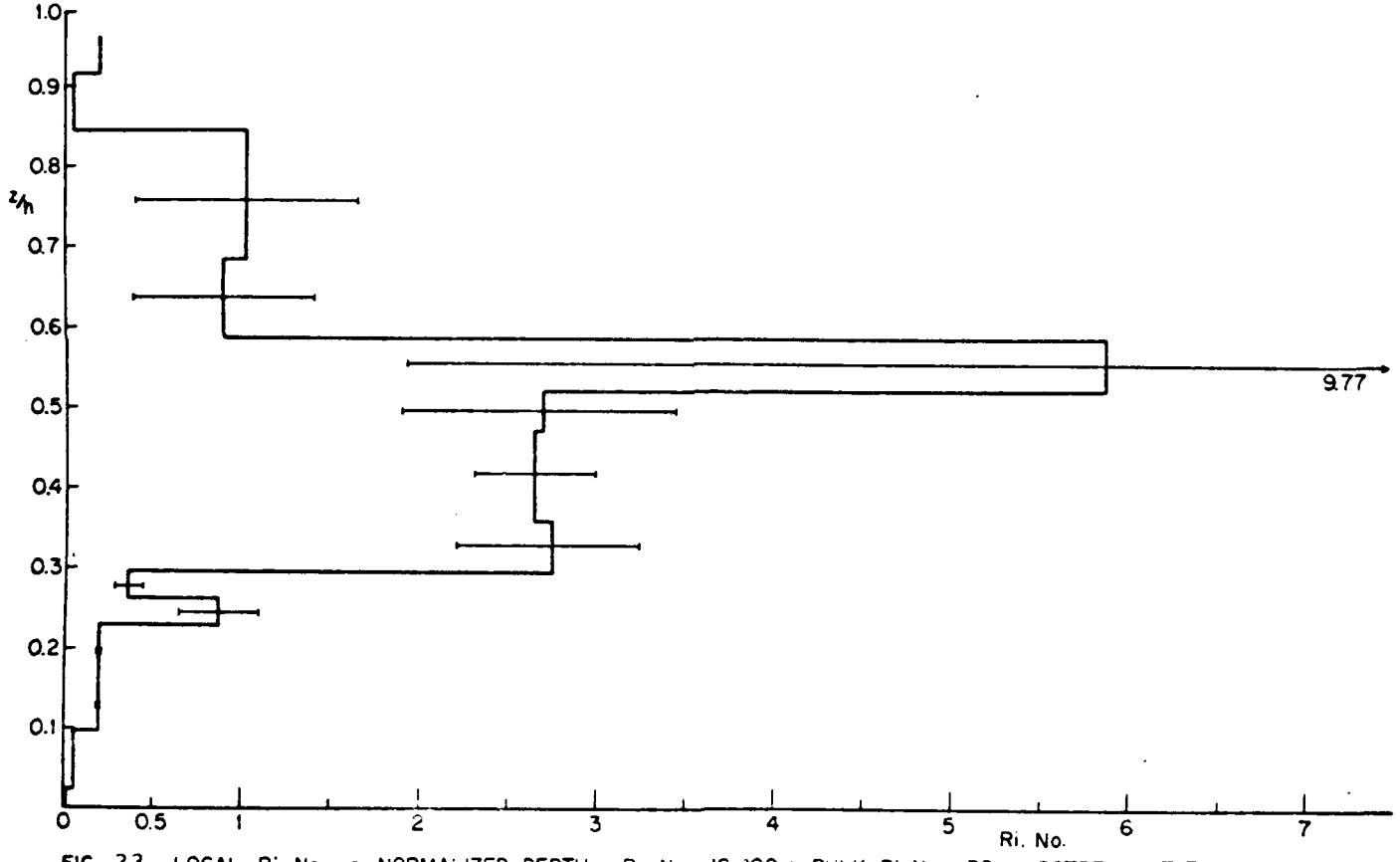

FIG. 33 LOCAL Ri. No. vs. NORMALIZED DEPTH. Re. No. = IC.XOO ; BULK Ri. No. = .38 ; UPSTREAM STATION 2

TABLE 1

Contributions to the Momentum and Salinity Fluxes from the

Various Terms in the Equations of Motion

$\left(\frac{z}{h}\right)$	$\tau(z)$ $\frac{cm^2}{sec^2}$	Term 1 τ_w	Term 2 $\frac{1}{\rho_0}\frac{\Delta P}{\Delta L}z$	Term 3	Term 4	Term 5	Term 6	$g_s(z/h)$ $\frac{cm}{sec}$ $\times 10^3$	Term 1	Term 2
.0033	.237	.24	-.0032	$.833\times10^{-4}$	$-.833\times10^{-4}$	$-.56\times10^{-4}$	$.25\times10^{-4}$	-.0025	$-.827\times10^{-4}$	$.802\times10^{-4}$
.0121	.228	.24	-.0116	$.797\times10^{-3}$	$-.576\times10^{-3}$	$-.105\times10^{-2}$	$.56\times10^{-3}$	-.0172	$-.473\times10^{-3}$	$.454\times10^{-3}$
.0233	.217	.24	-.0222	$.247\times10^{-2}$	$-.153\times10^{-2}$	$-.481\times10^{-2}$	$.28\times10^{-2}$	-.0464 -.389	$-.123\times10^{-2}$ -.0159	$.118\times10^{-2}$ .0156
.0618	.085	.24	-.0591	.0166	-.0116	-.193	.0912	-.467	-.0204	.0200
.128	.065	.24	-.1227	.0366	-.0137	-.290	.215	-.403	-.0241	.0237
.194	.029	.24	-.186	.0467	-.0048	-.399	.332	-.378	-.0251	.0247
.244	.019	.24	-.234	.0517	+.0021	-.433	.392	-.323	-.0262	.0259
.278	.0094	.24	-.266	.0511	.0097	-.476	.432	-.191	-.0238	.0236
.328	.020	.24	-.313	.0442	.0259	-.398	.422	-.082	-.0176	.0185
.420	.061	.24	-.402	.0336	.0490	-.212	.352	-.067	-.0162	.0161
.499	.050	.24	-.477	.0296	.0593	-.120	.318	-.035	-.0131	.0130
.554	.047	.24	-.530	.0253	.0669	+.0025	.263	+.019	-.00630	.00628
.637	.134	.24	-.609	.0204	.0756	.277	.130	+.063	$-.334\times10^{-3}$	$.445\times10^{-3}$
.757	.135	.24	-.735	.0175	.0826	.520	.0093	+.063	+.00160	.00153
.873	.074	.24	-.841	.020	.0826	.605	.033	+.063	.00212	.00205
.935	.031	.24	-.896	.0213	.0826	.626	.044			

Downstream Station 4

Ri. No. = .33, Re. No. = 10,000

TABLE II

Comparison of the Molecular and Turbulent Salinity and Momentum Fluxes and Austausch Coefficients

z/h	$\nu \frac{\Delta u}{\Delta z}$ $\frac{cm^2}{sec^2}$	$\frac{\Delta u}{\Delta z}$ $\frac{1}{sec}$	$\lambda_s \frac{\Delta \rho}{\Delta z}$ $\frac{cm}{sec}$ $\times 10^7$	$\frac{\Delta \rho}{\Delta z}$ $\frac{1}{cm}$	$-\overline{u'w'}$ $\frac{cm^2}{sec^2}$	$+\overline{\rho' w'}$ $\frac{cm}{sec}$ $\times 10^5$	K_m $\frac{cm^2}{sec}$ $\times 10^2$	K_s $\frac{cm^2}{sec}$ $\times 10^3$
.033	.240	24.6	.420	.0035	.0033	.25	.01	.74
.0121	.240	24.6	.25	.0020	.012	1.74	.05	8.7
.0233	.240	24.6	.25	.0020	.023	4.64	.09	23.3
.0618	.202	20.7	1.64	.0130	.117	34.5	.56	26.5
.128	.122	12.5	2.40	.0190	.056	46.7	.45	24.6
.194	.095	9.7	2.17	.0172	.065	40.3	.67	23.4
.244	.055	5.6	2.23	.0176	.036	37.8	.63	21.4
.278	.069	7.1	2.16	.0170	.079	32.3	1.1	19.0
.329	.035	3.6	1.94	.0153	.015	19.2	.42	12.6
.420	.020	2.1	1.89	.0150	.041	8.23	1.2	5.5
.499	.018	1.8	1.46	.0115	.032	6.71	1.77	5.8
.554	.015	1.5	.62	.0049	.052	3.66	3.48	7.3
.637	.003	.82	.23	.0018	.2259	-1.83	17.43	
.757	.003	.53	.08	.0007	.1322	-6.1	25.02	
.878	.016	1.63	.02	.0002	.058	-6.1	3.54	
.935	.0025	.26	.06	.0005	.028	-6.1	10.9	

Downstream Station 4

Re. No. = 10,000

Ri. No = .33

$\nu = .0118$ cm²/sec

$\lambda_s = 1.46 \times 10^{-5}$ cm²/sec

TABLE III

Bulk Ri. No. vs Stress at the Wall

	Ri. No. = .38	.367	.35	.33	.30	.22	Re. No.
Run 1 τ_w				.331			9,600
Run 2 τ_w						.381	11,900
Run 3 τ_w		.290			.260		9,400
Run 4 τ_w	.275		.240				10,000

Upstream ——————→ Downstream

τ_w Units in $\frac{gm}{sec^2}$

APPENDIX I

Requirements for a Steady State Flow in the Neutral Case Using a Logarithmic Velocity Profile

The geometry of the flow is:

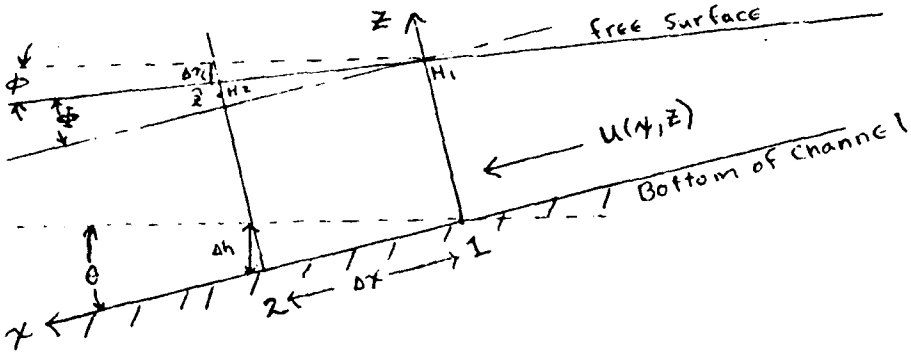

From continuity we have:

$$(1)\quad \int_0^{H_1} u(x,z)\,dz = \int_0^{H_2} u(x+\Delta x, z)\,dz = \int_0^{H_1} u(x+\Delta x, z)\,dz + \int_{H_1}^{H_1+\Delta H} u(x+\Delta x, z)\,dz$$

and

$$(2)\quad -\Delta x \int_0^{H_1} \frac{\partial u}{\partial x}\,dz = u(x+\Delta x, \hat{z})\,\Delta H$$

where $\hat{Z}$ is the point of the mean velocity between H_1 and H_2 at $x + \Delta x$.

$$(3)\quad u(x+\Delta x, \hat{z})\,\Delta H = u(x, H_1)\,\Delta H + \frac{\partial u(x,H_1)}{\partial x}\Delta x\,\Delta H + \frac{\partial u(x,H_1)}{\partial z}(\hat{z}-H_1)\,\Delta H$$

combining (2) and (3) we have,

$$(4)\quad \int_0^{H_1} \frac{\partial u}{\partial x}\,dz = u(x,H_1)\frac{\Delta H}{\Delta x} + \frac{\partial u}{\partial x}\Delta H + \frac{\partial u}{\partial z}(\hat{z}-H_1)\frac{\Delta H}{\Delta x}$$

To first order we then have,

$$(5)\quad \int_0^H \frac{\partial u}{\partial x}\,dz = U(x,H)\frac{\partial H}{\partial x}$$

The momentum equations are:

$$(6)\quad U\frac{\partial u}{\partial x} + \frac{\partial \overline{u^2}}{\partial x} + W\frac{\partial u}{\partial z} + \frac{1}{\rho}\frac{\partial p}{\partial x} = g\sin\theta + \frac{\partial}{\partial z}\overline{uw} = g\sin\theta + \frac{\partial}{\partial z}\tau(z)$$

$$(7)\quad \frac{1}{\rho}\frac{\partial p}{\partial z} = -g\cos\theta$$

Integrating equation (7),

$$(8)\quad p(x,z) = p_0 + g\cos\theta(H-z) \quad \text{where } p_0 = \text{surface pressure}$$

and

$$(9)\quad \frac{\partial p}{\partial x} = g\cos\theta\frac{\partial H}{\partial x}$$

equations (6) and (9) yield

$$(10)\quad U\frac{\partial u}{\partial x} + \frac{\partial \overline{u^2}}{\partial x} + W\frac{\partial u}{\partial z} + g\cos\theta\frac{\partial H}{\partial x} - g\sin\theta = \frac{\partial}{\partial z}\tau(x,z)$$

Now:

$$\tan\phi = \frac{\partial H}{\partial x} = \tan(\theta-\phi) = \frac{\tan\theta - \tan\phi}{1+\tan\theta\tan\phi} \approx \tan\theta - \tan\phi$$

$$\tan\phi = \frac{\partial h/\partial x - \partial z_c/\partial x}{1 - \partial h/\partial x\,\partial z_c/\partial x} \approx \frac{\partial h}{\partial x} - \frac{\partial z_c}{\partial x} \quad \text{for small angles}$$

Thus equation (10) becomes

$$(11)\quad U\frac{\partial u}{\partial x} + \frac{\partial \overline{u^2}}{\partial x} + W\frac{\partial u}{\partial z} + g\cos\theta\left(\frac{\partial H}{\partial x} - \tan\theta\right) = \frac{\partial}{\partial z}\tau(x,z)$$

$$(12)\quad U\frac{\partial u}{\partial x} + \frac{\partial \overline{u^2}}{\partial x} + W\frac{\partial u}{\partial z} + g\frac{\partial z_c}{\partial x} = \frac{\partial}{\partial z}\tau(x,z)$$

Using the continuity equation:

$$(13)\quad \frac{\partial u}{\partial x} + \frac{\partial w}{\partial z} = 0$$

and integrating from 0 to H, equation (12) becomes

$$(14)\quad \int_0^H \frac{\partial}{\partial x}(u^2 + \overline{w'^2})dz + uw\Big|_0^H + g\frac{\partial \eta}{\partial x}H = \tau_s - \tau_w \approx -\tau_w$$

Now as $\quad w(x,H) = u_{surface}\frac{\partial H}{\partial x}$ and as $\frac{\overline{w'^2}}{u^2} << 1$

We have

$$(15)\quad \int_0^H \frac{\partial u^2}{\partial x}dz + u_s^2\frac{\partial H}{\partial x} + g\frac{\partial \eta}{\partial x}H = -\tau_w$$

Letting,

$$u = u_*\left(\frac{1}{k}\ln\frac{u_* z}{\nu} + A\right) \quad \text{and} \quad u_s = u_*\left(\frac{1}{k}\ln\frac{u_* H}{\nu} + A\right)$$

we have:

$$(16)\quad H\frac{\partial u_*^2}{\partial x}\left[\left(\frac{u_s}{u_*}\right)^2 - \frac{1}{k}\frac{u_s}{u_*} + \frac{1}{k^2}\right] + u_s^2\frac{\partial H}{\partial x} + g\frac{\partial \eta}{\partial x}H = -\tau_w$$

Using equation (5) $\quad \int_0^H \frac{\partial u}{\partial x}dz = u_s\frac{\partial H}{\partial x} = \frac{\partial}{\partial x}u_*\int_0^H\left(\frac{1}{k}\ln\frac{u_* z}{\nu} + A\right)dz$

we have

$$(17)\quad \left[1 - \frac{\overbrace{u_s^2}^{\text{Fr. No.}}}{gH}\frac{\partial \eta/\partial x - \partial h/\partial x}{\partial \eta/\partial x}\left\{1 - \frac{2u_*}{ku_s} + \frac{2u_*^2}{k^2u_s^2}\right\}\right]\frac{1}{\rho}\frac{\partial P}{\partial x}H = -\tau_w$$

Where the value of the brackets $\{\ \}$ is nearly constant at 0.78. Laufer, ref 15, found the ratio of $\frac{u_*^2}{u_s^2} = .0018$ for all Re.Nos. The value here is .0020

Using the data from figure 10

The measured wall stress, $\tau_w = .0056\ ft^2/sec^2$

and $H = .141$ ft

Fr. No. $= .619$ $\qquad k = .41$

$\frac{\Delta \eta}{\Delta x} = 10.3 \times 10^{-4}$ $\qquad u_* = .0747$ ft/sec

$\frac{\Delta h}{\Delta x} = 14.1 \times 10^{-4}$ $\qquad \frac{1}{\rho}\frac{\Delta P}{\Delta x} H = .0048\ ft^2/sec^2$

Thus: $1.18 \frac{1}{\rho}\frac{\Delta P}{\Delta x} H = -\tau_w$

$-.00569 \simeq -.00560$

The corrected pressure gradient balances τ_w.

Using the data from figure 11:

$\tau_w = .0073\ ft^2/sec^2$, $\frac{1}{\rho}\frac{\Delta P}{\Delta x} H = .00758\ ft^2/sec^2$

Fr. No. $= .962$, $\frac{\Delta \eta}{\Delta x} = -19.5 \times 10^{-4}$, $\frac{\Delta h}{\Delta x} = -20.5 \times 10^{-4}$

Thus: $.963 \frac{1}{\rho}\frac{\Delta P}{\Delta x} H = -\tau_w$ and

$.00730 \simeq .00730$

Thus, by tilting the channel the flow is steady state.

APPENDIX II

Preliminary Mean and Fluctuating Velocity Profiles at Various Richardson Numbers

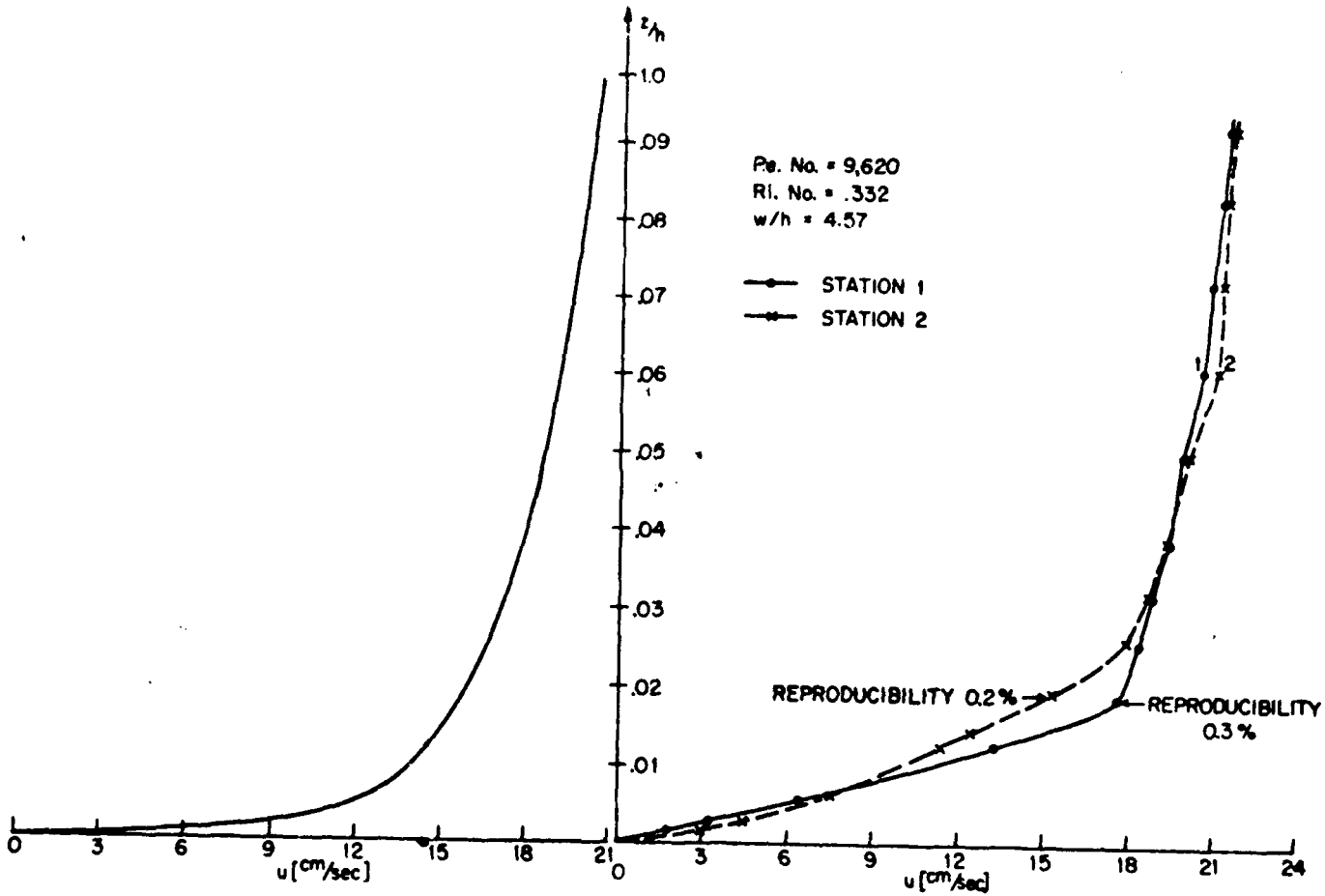

MEAN VELOCITY vs. DEPTH - NEUTRAL CONDITIONS

MEAN VELOCITY vs. DEPTH

FIG. II-1

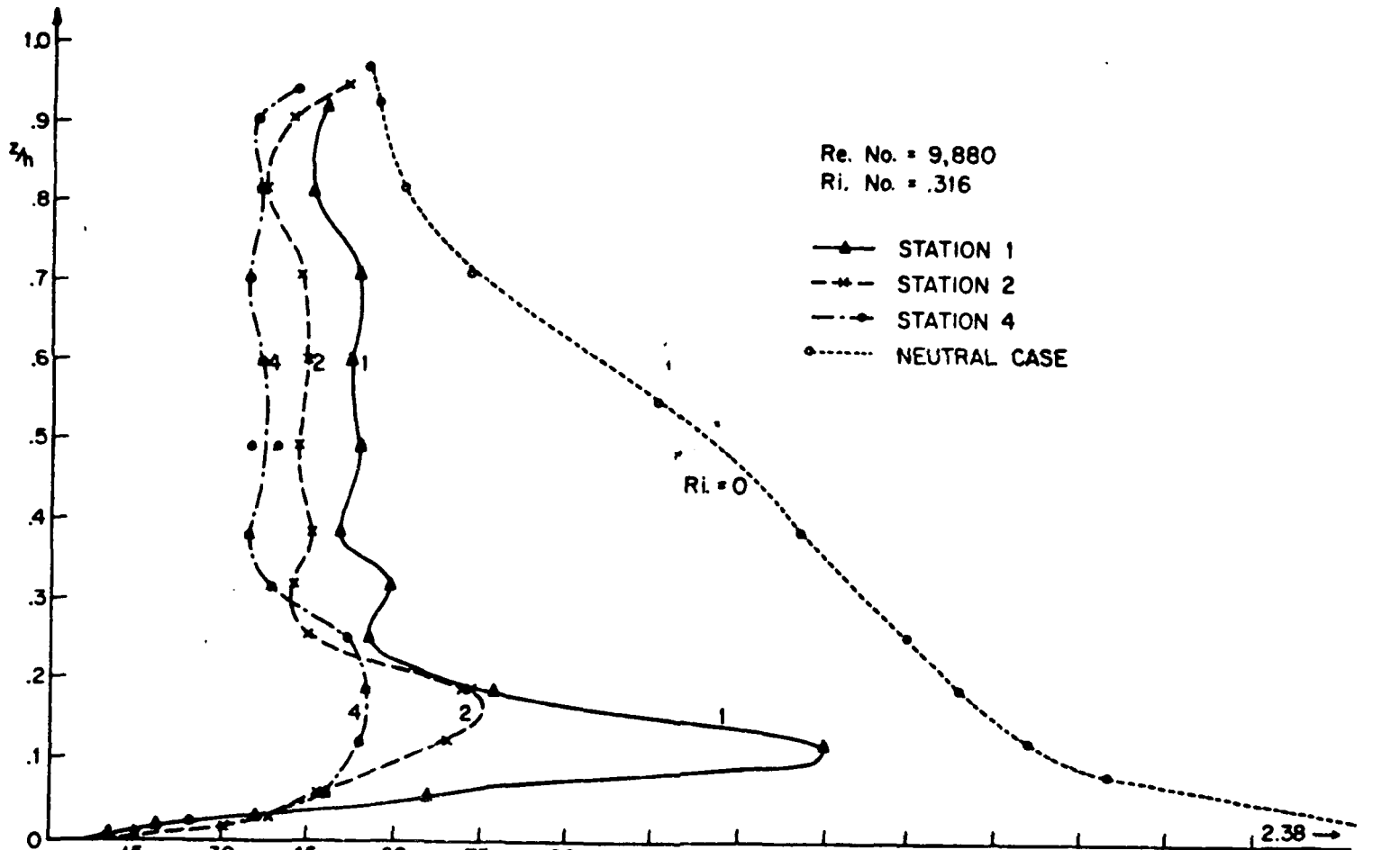

FIG II-2 RMS FLUCTUATING VELOCITY vs. DEPTH

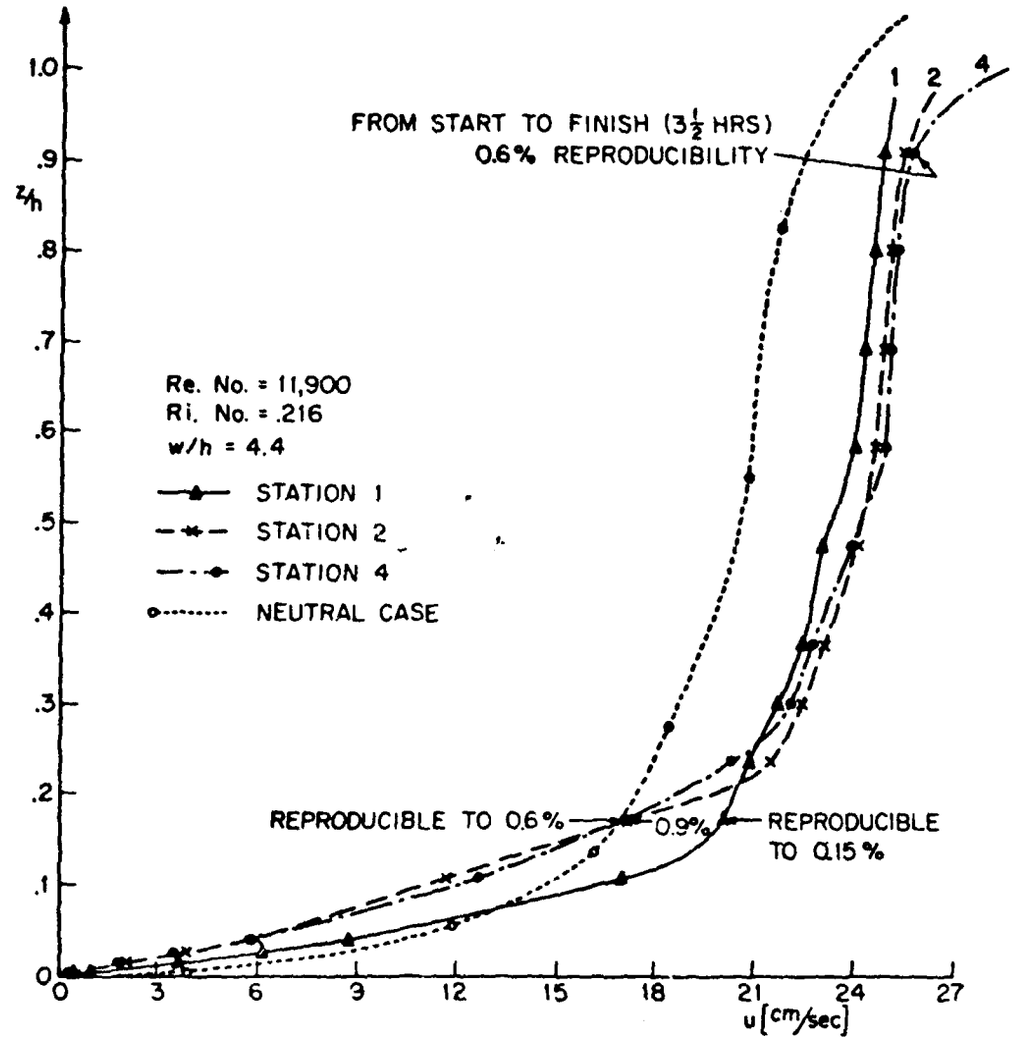

II-3 MEAN VELOCITY vs. DEPTH

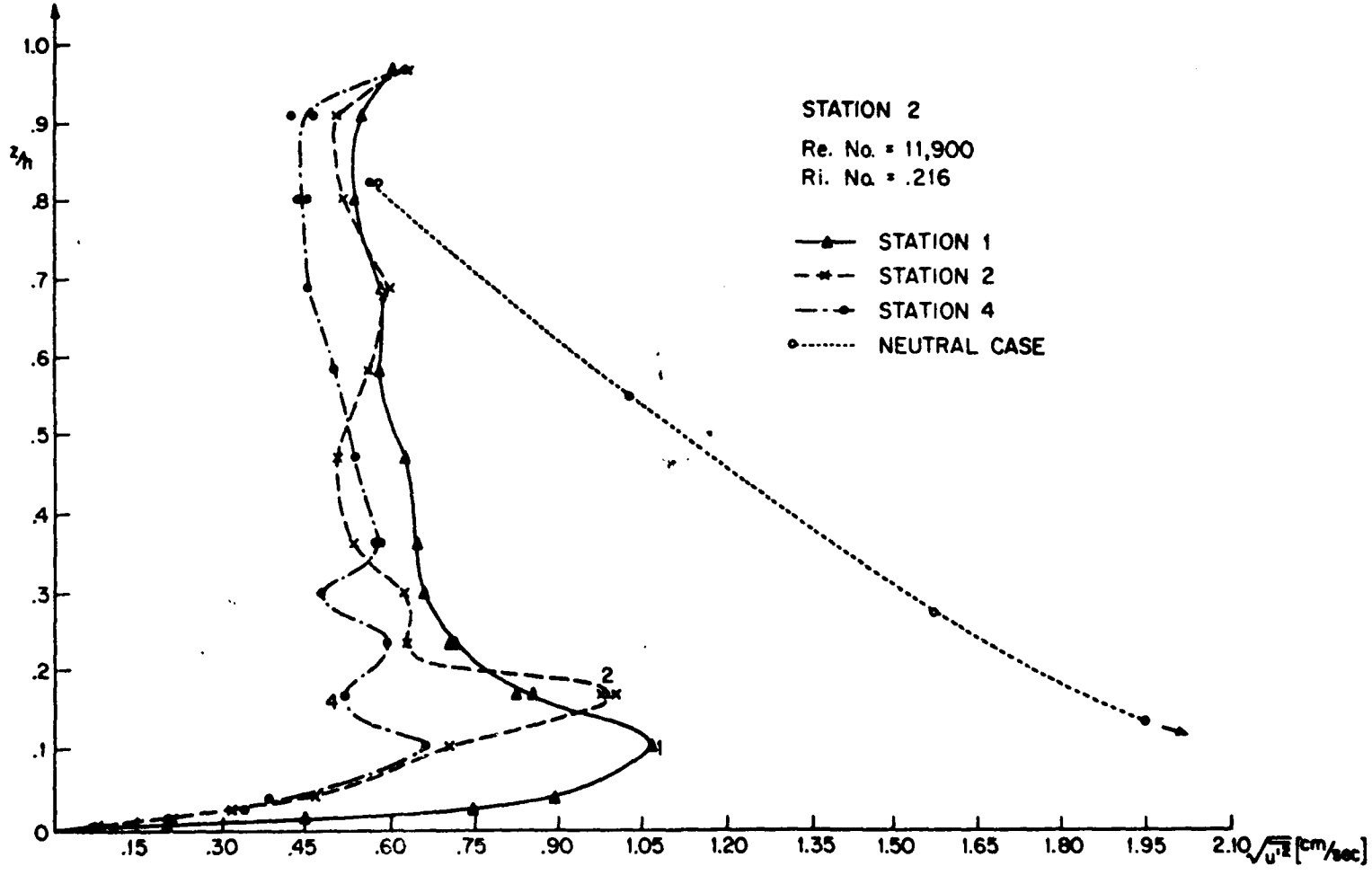

FIG. II-4 RMS FLUCTUATING VELOCITY vs. DEPTH